Search for a RPV resonance in the $\mu\tau$ final state at CMS

von
Malte Neul

Bachelorarbeit in Physik

vorgelegt der
Fakultät für Mathematik, Informatik und Naturwissenschaften der
RWTH Aachen

angefertigt am
III. Physikalischen Institut A

im
August 2016

bei
Prof. Dr. Thomas Hebbeker

Eidesstattliche Versicherung

Name, Vorname

Matrikelnummer (freiwillige Angabe)

Ich versichere hiermit an Eides Statt, dass ich die vorliegende Arbeit/Bachelorarbeit/ Masterarbeit* mit dem Titel

selbständig und ohne unzulässige fremde Hilfe erbracht habe. Ich habe keine anderen als die angegebenen Quellen und Hilfsmittel benutzt. Für den Fall, dass die Arbeit zusätzlich auf einem Datenträger eingereicht wird, erkläre ich, dass die schriftliche und die elektronische Form vollständig übereinstimmen. Die Arbeit hat in gleicher oder ähnlicher Form noch keiner Prüfungsbehörde vorgelegen.

Ort, Datum

Unterschrift

*Nichtzutreffendes bitte streichen

Belehrung:

§ 156 StGB: Falsche Versicherung an Eides Statt

Wer vor einer zur Abnahme einer Versicherung an Eides Statt zuständigen Behörde eine solche Versicherung falsch abgibt oder unter Berufung auf eine solche Versicherung falsch aussagt, wird mit Freiheitsstrafe bis zu drei Jahren oder mit Geldstrafe bestraft.

§ 161 StGB: Fahrlässiger Falscheid; fahrlässige falsche Versicherung an Eides Statt

(1) Wenn eine der in den §§ 154 bis 156 bezeichneten Handlungen aus Fahrlässigkeit begangen worden ist, so tritt Freiheitsstrafe bis zu einem Jahr oder Geldstrafe ein.

(2) Straflosigkeit tritt ein, wenn der Täter die falsche Angabe rechtzeitig berichtigt. Die Vorschriften des § 158 Abs. 2 und 3 gelten entsprechend.

Die vorstehende Belehrung habe ich zur Kenntnis genommen:

Ort, Datum

Unterschrift

Abstract

This bachelorthesis is about the search for a resonant, lepton number violating decay of a tau sneutrino into the $\mu\tau$ final state. Only tau leptons which decay hadronically are taken into account. This is done using 2015 CMS data with a center-of-mass energy of 13 TeV and an integrated luminosity of 2.7 fb^{-1}. Different types of tau discriminators are studied and various kinematic cuts are applied to optimize the signal to background ratio. As there is no sign for non standard model processes in the final invariant $\mu\tau$-mass distribution, a limit on the tau sneutrino mass is calculated.

Zusammenfassung

Diese Bachelorarbeit befasst sich mit der Suche nach resonanten, leptonenzahlverletzenden Zerfällen des Tau Sneutrinos in ein Muon und ein Tau. Dabei werden nur Tau Leptonen betrachtet welche hadronisch zerfallen. Benutzt werden dafür Daten vom CMS Detektor, aufgenommen im Jahr 2015 bei einer Schwerpunktsenergie von 13 TeV und einer integrierten Luminosität von 2.7 fb^{-1}. Verschiedene Tau Diskriminatoren werden untersucht und mehrere kinematische Schnitte optimiert um das Verhältnis von Signal zu Untergrundereignissen zu verbessern. Da in der finalen $\mu\tau$-Massenverteilung kein Hinweis für eine Abweichung vom Standardmodell zu sehen ist, wird eine Auschlussgrenze für die Tau-Sneutrino Masse errechnet.

Contents

1 Introduction **1**

2 Theoretical Background **3**
2.1 Standard Model of Particle Physics 3
2.1.1 Motivation for beyond SM Theories 5
2.2 Supersymmetry 6
2.2.1 General Idea 6
2.2.2 R-Parity Violation 7

3 Overview on CMS **9**
3.1 The detector 9
3.2 Important quantities 11

4 Event selection **13**
4.1 Trigger 13
4.2 Muon identification 13
4.3 Tau identification 14
4.4 Event selection 15

5 Dataset and Monte Carlo Samples **17**
5.1 Dataset 17
5.2 Signal simulation 17
5.3 Background simulation 18
5.3.1 Prompt background 18
5.3.2 Fake backgrounds 21

6 Analysis **25**
6.1 Discriminators 25
6.2 Mass Resolution 28
6.3 Signal Efficiency 30
6.4 Systematics 32
6.5 Limit calculation 32
6.6 Kinematic Cuts 32

7 Result **41**

8 Conclusion 43

9 Appendix 45

Bibliography 49

1 Introduction

Different experiments have shown, that there are various effects which can not be described by the Standard Model of Particle Physics. Therefore new theories are needed to extend the current model. Some of these theories, capable of solving some of the problems of the Standard Model, were created tens of years ago, but are still waiting for experimental proof. The LHC, as current most powerful particle accelerator, now gives us a chance to search for evidences of those theories.

Extending the Standard Model, the supersymmetric theory is able to solve some of its problems. The $\tilde{\nu}_\tau$ is the supersymmetric partner to the Standard Model ν_τ, introduced by the minimal supersymmetric model. As the lightest supersymmetric particle, the $\tilde{\nu}_\tau$ decays into Standard Model particles, which can be observed. These decays violate the empiric found lepton number conservation.

For the 13 TeV data a first look at the $e\mu$ final state was done, as these particle are easy to reconstruct. Another possible decay mode is given by $\tilde{\nu}_\tau \to \mu\tau$. This channel is more difficult to study, as the tau lepton got a extreme short lifetime and therefore decays in the detector. If the tau decays into a lepton, different reconstruction effects have to be taken in account in comparison of the tau decaying hadronically. Therefore only hadronic decaying taus are studied. The aim of this analysis is to take a first look at the $\mu\tau_h$ channel for the $\sqrt{s} = 13\,\text{TeV}$ data. This is done using 2015 CMS data with a integrated luminosity of about $2.7\,\text{fb}^{-1}$.

2 Theoretical Background

In this chapter a short overview over the Standard Model, its problems and the addition of a minimal supersymmetric model is given. The chapter is based on Ref. [1] and Ref. [2].

2.1 Standard Model of Particle Physics

The Standard Model of Particle Physics (SM) is a theory that combines our current knowledge about all elementary particles and their interactions. It includes the description of the three particles which make up all matter: The electron, the up quark and the down quark. Also there are additional groups of unstable subatomic particles. All particles, which have half integer spin, are grouped together as fermions and are furthermore separated into leptons and quarks, depending on their interactions. In addition there are particles with an integer spin, called bosons, which are the mediators of the forces. For each SM particle there is also a corresponding antiparticle with the same mass but opposite sign in all charge-like quantities.

Leptons and quarks are divided into three generations, which are stacked up by the mass of their particles, so each member of a special generation is heavier then all particles of lower generations. Therefore particles can only decay into lower generations or, if the partner particle is lighter, within their generation as other decays violets energy conservation. This does not apply for neutrinos, as they do not decay. The first generation is considered to be stable, as no decay has been measured yet.
There are six different leptons, three charged ones and corresponding to each charge one an uncharged, massless neutrino. The charged leptons, namely the electron, the muon and the tau, participate in the electromagnetic interaction and in the weak one, as they also carry a weak isospin. Neutrinos only interact weakly because they carry a weak isopsin and are electrically neutral. Both charged leptons and neutrinos do not carry a color charge and therefore do not participate in the strong interaction. In addition each lepton generation got an charge-like property called lepton number. All particles of a single lepton generation got a generational lepton number of 1 while all other particles got 0. So, for example, a electron and electron neutrino got an electron number of 1 but a muon and tau number of 0. Additionally all corresponding antiparticles got the same lepton number but with reversed sign.

In the SM the generational leptons numbers are conserved quantities. An overview about the mass and charge of each lepton is given in Tab. 2.1.

Tab. 2.1: The three lepton generations of the SM with their corresponding mass and electric charge [3]

Generation	Name	Symbol	Mass (eV)	Charge (e)
1	electron	e	$511 \cdot 10^3$	-1
	electron neutrino	ν_e	< 2	0
2	muon	μ	$106 \cdot 10^6$	-1
	muon neutrino	ν_μ	$< 0.19 \cdot 10^6$	0
3	tau	τ	$1776 \cdot 10^6$	-1
	tau neutrino	ν_τ	$< 18 \cdot 10^6$	0

The six different quarks are: Up, down, charm, strange, top, bottom. In each generation there is a quark with electric charge ⅔ e and one with charge - ⅓ e. As they carry color charge as well as an electric one and a weak isospin, quarks participate in the electromagnetic, the weak and the strong interaction. Also each quark got an additional charge-like quantity called baryon number of ⅓ respectively - ⅓ for antiquarks. Similar to the lepton number, the baryon number is also a conserved property in the SM. In Tab. 2.2 an overview about the masses and the charges of the different quarks is given.

Tab. 2.2: The three quark generations of the SM with their corresponding mass and electric charge [3]

Generation	Name	Symbol	Mass (eV)	Charge (e)
1	up	u	$2.3 \cdot 10^6$	+ ⅔
	down	d	$4.8 \cdot 10^6$	- ⅓
2	charm	c	$1.3 \cdot 10^9$	+ ⅔
	strange	s	$95 \cdot 10^6$	- ⅓
3	top	t	$173 \cdot 10^9$	+ ⅔
	bottom	b	$4.2 \cdot 10^9$	- ⅓

The gauge bosons are the mediators of the elementary forces, as an interaction is described as an exchange of particles in the SM. There are three different elementary forces in the SM: Electromagnetic, weak and strong. A fourth force, gravitation, is known but not part of the SM. Each force got its own mediators.
The photon is the massless mediator of the electromagnetic force between two electrically charged particles. This interaction is described by the Quantum Electrodynamics (QED) and is by the factor 1/137 weaker compared to the strong interaction. The gluon is the massless mediator of the strong force between two particle with a color charge, the corresponding theory is the Quantum Chronodynamics (QCD). In contrast to the other mediators, a gluons carrys a color charge itself in the form of one color (red, green, blue) and one anticolor (antired, antigreen, anitblue). This

would lead to 9 different gluons, but du to the singlet state not existing, there are only 8 different gluons. As a charged mediator, the gluons can couple to themself. If quarks bound by gluons get separated by force (for example during a proton-proton collision) their potential energy increases until a new quark antiquark pair arises. This effect appears because the potential of the strong force becomes linear for high distances. The new pair and the existing quarks then form colorless particles, the hadrons. There are two forms of hadrons: Mesons, consisting of a quark-antiquark pair and baryons, made up by three quarks. Therefore particles with color charge are not detected isolated, which is called confinement.
Coupling to the weak isospin, the mediators of the weak interaction are the massive Z and $W^{\pm}$ particles. Caused by the high mass of the force mediators, the strength of the weak interaction in comparison to the other two forces is relatively small: The strong force is 10^6 times stronger then the weak one. Only the weak force, described by the Quantum Flavor Dynamics (QFD), is able to change the flavor of a particle.

All particles in the SM need to be massless, as massive particles lead to a break in the gauge symmetry. To solve this discrepancy a theory called higgs-mechanism was introduced. In this theory a Higgs boson couples to the fermions and massive bosons and therefore gives them their mass. With the discovery of the Higgs boson in 2012 [4], this theory seems to be validated. All gauge bosons are shown in Tab.2.3.

Tab. 2.3: The different gauge bosons as mediators of the three elementary forces of the SM, with their corresponding mass and electric charge [3]

Name	Symbol	Mass (eV)	Charge (e)	Interaction
Photon	γ	0	0	electromagnetic
Gluon	g	0	0	strong
W-Boson	$W^{\pm}$	$80 \cdot 10^9$	± 1	weak
Z-Boson	Z	$91 \cdot 10^9$	0	weak
Higgs	H	$126 \cdot 10^9$	0	Higgs

2.1.1 Motivation for beyond SM Theories

Although the SM is capable of correctly describing most physical processes, there are still several problems. As already mentioned, gravitation is not included and requires its own theory. Additionally the experimental discovery of neutrino oscillation [5] show that neutrinos have to have a mass greater zero, in direct contrast to the prediction of the SM. Another discrepancy between the SM and experimental measurements is given by evidences for the existence of dark matter. Cosmological observations of the rotational curves of galaxies show that they only consist to a small percentage out of visible mass. So there have to be additional particles in comparison to the current SM. An important, more theoretical, topic is the hierarchy problem.

Each lepton or quark coupling to the Higgs field causes quantum corrections, which would lead to a Higgs mass around 30 order of magnitude bigger then the mass of the observed Higgs boson [6]. To solve this the bare Higgs mass has to be chosen extreme precisely, which is the so called fine-tuning problem.
Because of these and other problems, there are a lot of different theories expanding the SM, which now need to be validated by experiments. In this thesis, parts of a special supersymmetric theory are discussed as a possible solution to some of these problems.

2.2 Supersymmetry

2.2.1 General Idea

The theory of supersymmetry introduces a new symmetry between fermions and bosons which changes the spin of a particle by 1/2 and therefore is capable of changing fermions into bosons and vice versa. In the minimal extension which is needed to make the SM supersymmetric, called minimal supersymmetric standard model (MSSM), each particle got exactly one supersymmetric partner or superpartner. The superpartner for each fermion is called sfermion, a short form for scalar fermion, and the superpartner of the bosons are given the suffix -ino (i.e. $e \rightarrow \tilde{e}$, $\nu_\mu \rightarrow \tilde{\nu}_\mu$, $H \rightarrow \tilde{H}$, etc.). All SM particles and their corresponding superpartner are shown in Tab. 2.4. In the MSSM the particles and their superpartners got identical quantum

Tab. 2.4: Supersymmetric partner of the SM particles and their spin, as introduced by the MSSM [7]. For each lepton there is a super symmetric boson and vice versa for every SM boson. As consequence of making the SM supersymmetric more then one supersymmetric partner to the Higgs boson is required. The different Higgs partners got either spin 0 or spin 1/2.

SM particle	Spin	Spin	Superpartner
lepton	1/2	1	slepton
quark	1/2	1	squark
gluons	1	1/2	gluino
W Boson	1	1/2	wino
B Boson	1	1/2	wino

numbers, except of the spin, and therefore need to have the same mass. As no such particles have been measured yet, the supersymmetrie is a broken symmetry. Also the MSSM theory presents explanations for various problems encountered by the SM: The lightest supersymmetric particle (LSP) is a stable and only weakly interacting particle and therefore a potential candidate for dark matter. In addition the hierarchy problem is solved, as the quadratic divergence in the correction of the higgs mass disappears. Another great success of the theory lays in the unification of the coupling constants of the three elementary forces in one single intersection

point, which is not possible in the SM as seen in Fig. 2.1. This is caused by the new supersymmetric particles, which distribute to the virtual corrections and therefore change the running of the coupling constants. As conclusion all forces described by the SM arise from one single force, which is necessary for a grand unified theory (GUT).

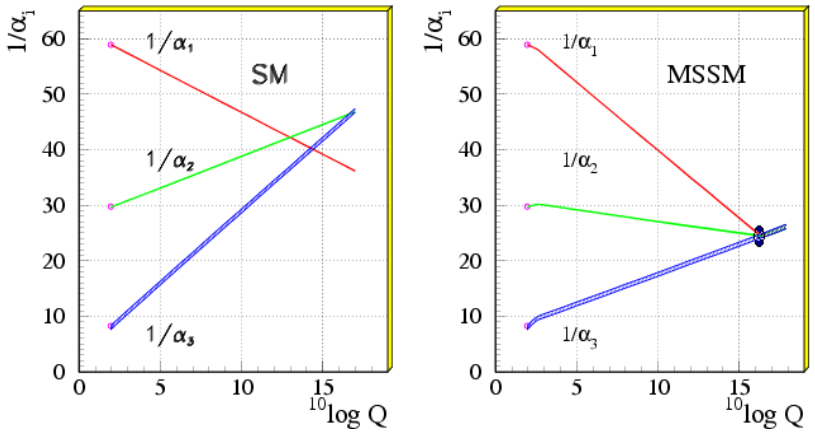

Fig. 2.1: Gauge couplings unification in non-SUSY GUTs on the left and in SUSY GUTs on the right [3]. Here the inverse coupling constants $1/\alpha_i$ are plotted as function of the logarithmic energy scale. The difference in the running is given by the inclusion of supersymmetric partners of SM particles in the scale of order a TeV.

2.2.2 R-Parity Violation

In some versions of supersymmetry lepton and baryon number violations are allowed, which in consequence lead to a proton lifetime not compatible with the experimental measured lower limit of around 10^{31} years [3]. Therefore a additional symmetry is introduced, the R-Parity [8]:

$$R = (-1)^{2S}\,(-1)^{3B+L} \tag{2.1}$$

The R-Parity is an additional multiplicative quantum number, consisting out of the baryon number B, the lepton number L and the spin S. In the MSSM R-Parity is a conserved number, as all SM particles got a R value of 1 and all added supersymmetric particles got a R value of -1. Therefore SM particles can only decay into SM particles and equally for the supersymmetric particles. As a consequence there has to be a lightest supersymmetric particle (LSP) which can not further decay. This particle is stable and only weakly interacting (if it does not carry charge) and therefore a candidate for dark matter.
In this thesis a R-Parity violating process is studied. Therefore an alternative theory is assumed to ensure the long lifetime of the proton. The baryon triality symmetry [9] forbids only baryon number violating processes, leaving lepton number violations

possible and stabilizes the proton. So the decay of a tau sneutrino ($\tilde{\nu}_\tau$), produced by quark-antiquark annihilation, into a tau and a muon is searched for. This is a R-Parity and lepton number violating process. The feynman diagram of this process is shown in Fig. 2.2.

The coupling λ' allows the annihilation of a quark-antiquark pair to a slepton. Due

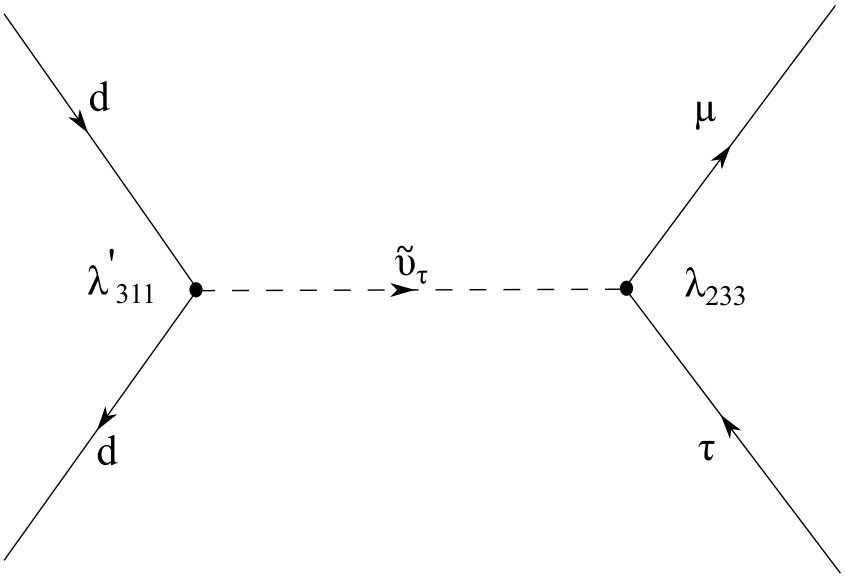

Fig. 2.2: Feynman diagram of the signal model. Here a quark antiquark pair annihilates, producing a tau sneutrino, which then decays into the final state of a muon and a tau, which is an R-Parity violating (RPV) process.

to the particle density function of the proton, the cross section for coupling to the first quark generation is the largest one. Therefore all couplings except of λ'_{311} will be set to zero and only the annihilation of $d\bar{d}$ into $\tilde{\nu}_\tau$ will be looked at. In addition we require the $\tilde{\nu}_\tau$ to decay into a muon and a tau. Therefore $\lambda_{233} = \lambda_{323} \neq 0$ has to be fulfilled. As there is no difference between a $\mu\bar{\tau}$ and a $\bar{\mu}\tau$ final state in the analysis, both couplings have to be taken in account. This are the only decay modes looked at in this thesis, the coupling of all other final states are set to 0.

3 Overview on CMS

In this chapter a short introduction over the structure of the CMS (Compact Muon Solenoid) detector, based on Ref. [10], is given.

3.1 The detector

CMS is one of the four big detectors (others are ATLAS, LHCb, ALICE) of the LHC (Large Hadron Collider), currently the world most powerful particle accelerator designed for proton-proton collisions at a center-of-mass energy of $\sqrt{s} = 14$ TeV and an luminosity of 10^{34} cm^{-2}s^{-1}. Build by CERN, the European Organization for Nuclear Research, the LHC is located in a 27 km long tunnel beneath the French-Swiss border. CMS itself is 21 m long, 15 m wide, 15 m high and weighs around 12500 tons. It is centred around the collision point and, as shown in Fig. 3.1, consists of different layers.

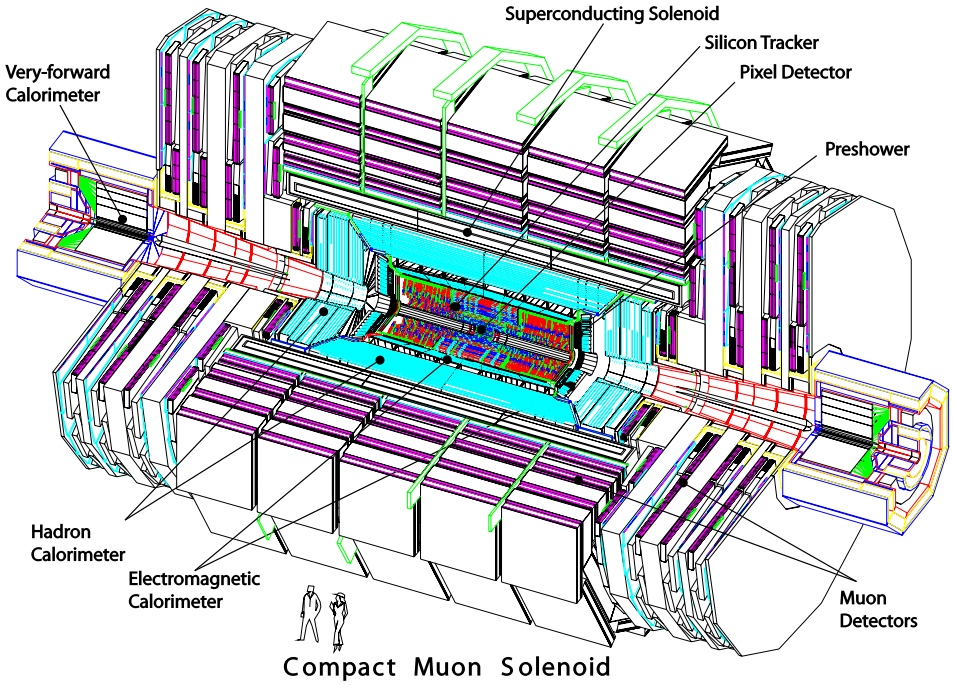

Fig. 3.1: A perspective view of the CMS detector, showing the different types of subdetectors: Inside of the superconducting solenoid, there are the silicon pixel and silicon strip detector, followed by the electromagnetic and hadronic calorimeter. Outside of the solenoid there are the muon chambers and the iron yoke [10].

The core part of CMS is a superconducting solenoid, which creates a magnetic field of 3.8 T. To confine the magnetic field, the outer part of the detector consists of an iron return yoke. Embedded into its homogeneous magnetic field, the inner tracking system records the trajectory of charged particles and measures their momentum. It consists of three inner barrel layers of silicon pixel detectors and additional ten outer barrel layers of silicon strip tracker. In the endcaps there are 2 disks in the pixel detector and 12 disks in the strip tracker on each barrel side. The inner layer got a pixel size of 100 x 150 μm^2 and due to his proximity to the collision point, is essential for the reconstruction of fast decaying particles like b quarks. For high momentum tracks (100 GeV) the transverse momentum resolution is around 1.5%.

The next outer layer is the electromagnetic calorimeter (ECAL), which measures the energy of electromagnetic interacting particles. It consists of over 75 000 lead tungstate ($PbWO_4$) crystals, used for their short radiation length. If an electron passes the ECAL, high energy photons are emitted as bremsstrahlung. These photons or photons produced in the collision, produce an electron/positron pair, which then again can produce bremsstrahlung, leading to a so called electromagnetic shower. The secondary particles also produce scintillation light, which can be measured by photodetectors to determine the energy of the primary particle. For electrons with an energy of 120 GeV an energy resolution of 0.5 % is archived.

The ECAL is surrounded by the hadronic calorimeter (HCAL). As the hadrons depose less energy per length in the crystals of the ECAL, another system has to be used to ensure a compact detector. Therefore the HCAL consists of alternating layers of absorption material and active scintillators. The hadrons interact in the absorber, made out of brass, and produce secondary particles, which then produce additional particle shower. This particles depose a part of their energy by flying through the plastic scintillator, producing photons which are measured via photodetectors.

The outer most part of CMS is the name giving muon system. The good momentum resolution is archived by the high magnetic field of the superconducting solenoid and the flux returning yoke. In addition the yoke serves as hadron absorber, ensuring that only muons, neutrons and neutrinos are capable of reaching this outer detector level. In the barrel region, where the magnetic field is uniform and the muon rate is low, rectangular drift cells are used. This barrel drift tubes (DT) are organized in 4 chambers, embedded between flux return plates. In the endcap regions cathode strip chambers (CSC) are used, due to the higher rate of muons and the larger, non uniform magnetic field. Additionally in both regions, barrel and the two endcaps, a complementary system of resistive plate chambers (RPC) was added. With the measurement of the trajectory, the momentum as well as the charge of a muon can be obtained by the bending of its trajectory. Combined with the inner tracker, both

detector parts together yield a momentum resolution of about 5% for high momenta (1 TeV) muons.

3.2 Important quantities

In the following section the most important quantities, which are regularly used in this thesis, are defined, as well as the coordinate system used by CMS. The origin of the coordinate system is placed in the nominal collision point inside the detector, the y-axis points vertically upward and the x-axis points radially inwards to the center of the LHC. In consequence the z-axis points along the beam pipe. A spherical coordinate convention is used, where ϕ is the azimuthal angle measured from the x-axis in the x-y plane and Θ is the polar angle measured from the z-axis. As further quantity the pseudorapidity η is introduced, which by convention is used instead of Θ. The definition of η is given by:

$$\eta = -\ln(\tan(\frac{\Theta}{2})) \tag{3.1}$$

In addition, as η and ϕ are orthogonal, the distance between two particles can be defined as ΔR in the following manner:

$$\Delta R = \sqrt{(\Delta\eta)^2 + (\Delta\phi)^2} \tag{3.2}$$

The momentum p_T and energy E_T transverse to the beam direction can be calculated using the x and y components.

$$p_T = p \cdot \sin(\Theta) \tag{3.3}$$

As the protons do not have a momentum orthogonal to the beam pipe before the collision, the sum of all p_T of the collision products have to be zero. Imbalances in this calculation can be come due to production of neutrinos or other undetected particles, which energy can not be measured, and is donated with E_T^{miss}.
As last important quantity the invariant mass M is introduced. This is defined as:

$$M = \sqrt{\left(\sum_i E_i\right)^2 + \left(\sum_i p_i\right)^2} \tag{3.4}$$

In this thesis a natural unit system is used, where $\hbar = c = 1$.

4 Event selection

The criteria which are used to identify detector signals as muon or tau leptons are given in this section. In addition the selection of events, which are taken in account for the further analysis, is described.

4.1 Trigger

Events were selected using a high energy single muon trigger, with a p_T threshold of 50 GeV.

4.2 Muon identification

For the selection of muon candidates, the high-p_T -muon ID is used, which is recommended for muons with $p_T > 200$ GeV [11]. The muon identification criteria are given by:

- The muon candidate has to be reconstructed as a global muon [12].
- At least one hit in the muon chamber has to be included in the global muon track fit, as well as the inner tracker need to have one or more hits in the pixel detector.
- The inner track needs to be matched to at least two track segments in the muon chambers.
- The relative p_T error of the muon best track needs to be smaller then 0.3.
- The transverse impact parameter with respect to the primary vertex d_{xy} has to be smaller then 0.2 cm and the longitudinal distance of tracker track with respect to the primary vertex d_z need to be smaller then 0.5 cm.
- There has to be at least 5 tracker layers containing a hit.

Additional offline cuts are implemented as suggested in [11] for the triggered muons: A $p_T > 53$ GeV is required as well as $|\eta| < 2.4$.

4.3 Tau identification

Tau leptons decay in 35 % [3] of cases leptonically to a muon or an electron and two neutrinos. The produced leptons are then reconstructed and identified as electron or muon. In the remaining cases, tau leptons decay hadronically mostly via ρ or a_1 resonance to a combination of charged and neutral mesons and one tau neutrino. The dominant decays are shown in Tab.4.1.

Tab. 4.1: Dominant hadronic tau decays with their branching ratio. $h^{\pm}$ stand for a charge hadron, either a pion or a kaon.

Decay mode	Meson resonance (MeV)	BR (%)
$\tau^- \to h^-\nu_\tau$		11.6
$\tau^- \to h^-\pi^0\nu_\tau$	$\rho(770)$	26.0
$\tau^- \to h^-\pi^0\pi^0\nu_\tau$	$a_1(1260)$	9.5
$\tau^- \to h^-h^+h^-\nu_\tau$	$a_1(1260)$	9.8
$\tau^- \to h^-h^+h^-\pi^0\nu_\tau$		4.8

Hadronic decaying tau leptons (τ_h) are reconstructed and identified with the Hadrons Plus Strips (HPS) algorithm [13]. As the most τ_h decays produce a neutral pion π^0, it is required to be reconstructed to specify the decay mode. The π^0 decays into a $\gamma\gamma$ pair, which then convert with a high probability to e^+e^- pairs. Therefore the electrons and photons of the possible τ-jet are clustered to "strips" in the η - ϕ plane in an iterative process. Here the electron or photon with the highest p_T is used as origin of a new strip. Then the electron or photon with the next highest p_T within the η - ϕ frame centred around the strip is merged into it and the η and ϕ of the strip is recalculated out of the energy-weighted averages of the electrons and photons contained in it. If no electron or photon is left inside the η - ϕ frame the construction of the strip ends and a new strip is created. If the p_T sum of all electrons and photons inside a strip is smaller then 2.5 GeV, the strip is discarded.
The τ_h candidates then are created by combining the charged particles of the jet with the strips. Then a combinatorial approach is used, where multiple τ_h hypothesis are taken in account. These hypothesis are corresponding to combinations of either on or three charged particles and either one or two strips for neutral pions. The hypothesis are discarded if they fail the mass window selection for the corresponding decay or got any strip or charged particle outside of a cone of $\Delta R = 3.0/p_T$ (GeV) around the momentum vector of the τ_h candidate. [14]

Furthermore different descriminators are applied to the τ_h candidate, reducing the effect of quarks or gluon jets, electrons or muons to be identified as hadronic tau. More details about the discriminators are given in sections 6.1.
In addition the τ_h candidates are required to have $p_T > 20$ GeV, to ensure the functionality of the HPS algorithm [15], and to have a $|\eta| < 2.3$ to be within the geometric acceptance.

4.4 Event selection

To be selected, the event is required to have at least one muon and one tau which pass the criteria defined above. As there is no information about the η of the neutrino, a colinear approximation is done: Thereby the E_T^{miss} is set to have the same polar angle as the visible part of the τ_h. Due to the high momentum of the tau leptons as result of the high mass of the $\tilde{\nu}_\tau$, the decay products are strongly boosted in one direction and inside a small ΔR cone, therefore the assumption of the polar angle is reasonable.
Only one $\mu\tau$ pair per event is selected, if there is more then one muon or tau, the pair with the highest invariant mass is chosen.

5 Dataset and Monte Carlo Samples

In this section an overview about the used data as well as the simulated background and signal samples is given.

5.1 Dataset

This analysis uses a dataset from the 2015 data taking period of CMS at a center-of-mass energy of $\sqrt{s} = 13\,\text{TeV}$ and an integrated luminosity of $2.7\,\text{fb}^{-1}$.

5.2 Signal simulation

Monte Carlo samples have been produced for the signal using the CalcHEP [16] generator. The signature of these signals is given by a resonance in the $M_{\mu\tau}$ spectrum. Different assumptions of the $\tilde{\nu}_\tau$ are simulated as shown in Tab. 5.1. All samples are produced with the couplings $\lambda'_{311} = \lambda_{233} = \lambda_{323} = 0.01$ and 15000 events each.

Tab. 5.1: Summary of simulated RPV signal samples with all used $\tilde{\nu}_\tau$ mass bins and the corresponding cross section times branching ratio.

$M_{\tilde{\nu}_\tau}$ (GeV)	$\sigma \cdot \text{BR}\,(\tilde{\nu}_\tau \to \mu^\pm\tau^\mp)$ (pb)	$M_{\tilde{\nu}_\tau}$ (GeV)	$\sigma \cdot \text{BR}\,(\tilde{\nu}_\tau \to \mu^\pm\tau^\mp)$ (pb)
200	0.59	1600	$0.27 \cdot 10^{-3}$
300	0.16	1800	$0.15 \cdot 10^{-3}$
400	$60 \cdot 10^{-3}$	2000	$87 \cdot 10^{-6}$
500	$28 \cdot 10^{-3}$	2500	$24 \cdot 10^{-6}$
600	$14 \cdot 10^{-3}$	3000	$7.1 \cdot 10^{-6}$
700	$8.2 \cdot 10^{-3}$	3500	$2.1 \cdot 10^{-6}$
800	$5.0 \cdot 10^{-3}$	4000	$6.4 \cdot 10^{-7}$
900	$3.1 \cdot 10^{-3}$	4500	$1.9 \cdot 10^{-7}$
1000	$2.1 \cdot 10^{-3}$	5000	$5.2 \cdot 10^{-8}$
1200	$0.97 \cdot 10^{-3}$	5500	$1.4 \cdot 10^{-8}$
1400	$0.49 \cdot 10^{-3}$		

5.3 Background simulation

The background can be separated into two different categories. One is the background with processes really producing a $\mu\tau$ final state, the other is given by processes which could be misidentified as events with a muon and a tau, called fake. A short overview about the most important backgrounds is given in the following sections, in addition all used Monte Carlo samples are shown in Tab. 9.1 (prompt) and Tab. 9.2 (fake) in the Appendix.

5.3.1 Prompt background

The backgrounds in this section are sorted by their contribution for low masses ($<$ 500 GeV). The contribution of all background processes for the different mass regions is given in Tab. 5.2.

Tab. 5.2: Contribution of the background process for different mass regions. For the low mass region ($<$ 1000 GeV), the background is mainly given by W+jets, $t\bar{t}$ and QCD. For the very low region ($<$ 500 GeV), Z$\rightarrow \mu\mu$ is also important. For hight masses, the background is dominated by W+jets events.

background process	0 - 500 GeV (%)	500 - 1000 GeV (%)
Diboson	5.1	5.5
DY$\rightarrow \tau\tau$	7.8	5.5
Z$\rightarrow \mu\mu$	19.2	3.0
$t\bar{t}$	22.2	27.2
Single top	2.7	3.7
W+jets	25.8	40.2
Z+γ / W+γ	3.0	1.7
QCD	14.2	13.2

background process	1000 - 1500 GeV (%)	1500-4000 GeV (%)
Diboson	2.9	9.5
DY$\rightarrow \tau\tau$	3.3	2.8
Z$\rightarrow \mu\mu$	3.2	1.6
$t\bar{t}$	10.9	4.0
Single top	0.7	2.1
W+jets	73.6	75.7
Z+γ / W+γ	3.2	4.3
QCD	2.2	0

Top / Antitop pair production

A top-antitop pair is produced and decays before it can hadronize, due to the short lifespan of the top quarks, into a b quark and a W boson. Both W bosons then decay leptonically, producing a similar final state as in the WW production, with the exception of two additional b-jets, shown in Fig. 5.1.

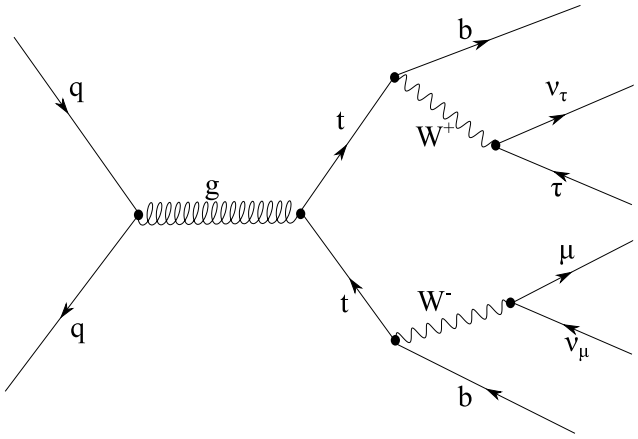

Fig. 5.1: Exemplary feynman diagram of the top/antitop pair production, where both W bosons decay leptonically.

Drell-Yan processes

A Z boson or a virtual γ is produced via quark-antiquark annihilation and then decays into two leptons of the same generation with opposite charge, shown in Fig. 5.2. If two tau leptons are produced, one can decay into a muon, a muon neutrino and a tau neutrino while the other decays hadronically, resulting in a $\mu\tau$ event.

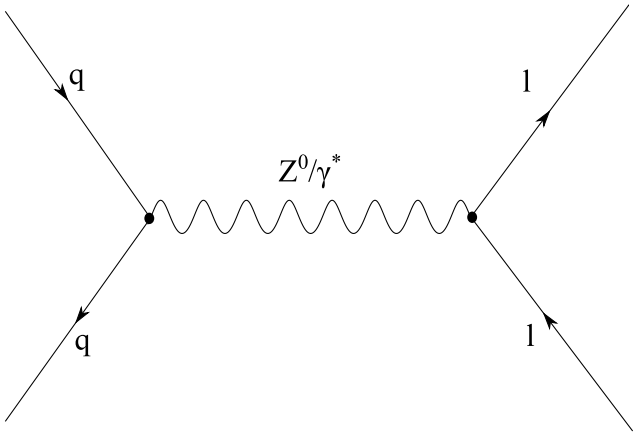

Fig. 5.2: Exemplary feynman diagram of the Drell-Yan process, where two quarks annihilate and emit a virtual photon / Z boson which then decays into a lepton antilepton pair.

W boson pair production

In this background process two W bosons are produced, both decaying leptonically. One decays into a muon and a muon neutrino, the other one into a tau and a tau neutrino. Muon and tau got different charges in this process, shown in the feynman diagram in Fig. 5.3. This background produces a $\mu\tau$ final state, with the two neutrinos.

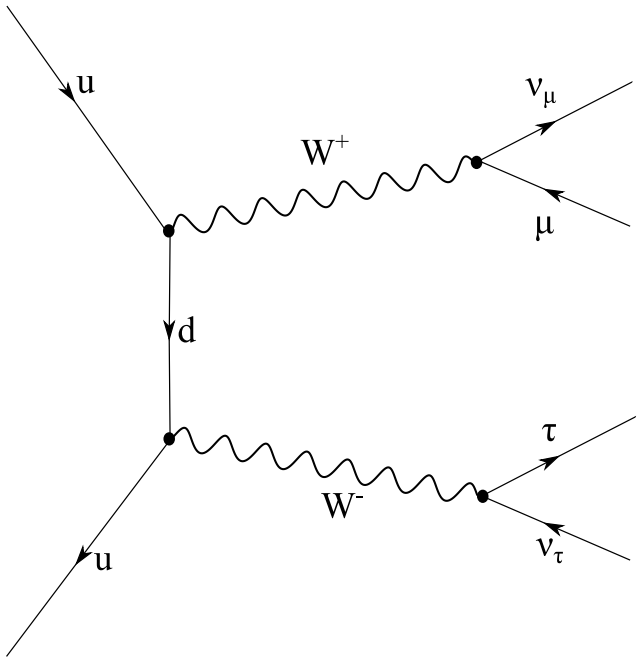

Fig. 5.3: Exemplary feynman diagram of the WW pair production, where both W bosons decay leptonically resulting in a $\mu\tau$ final state.

Diboson production including Z bosons

Analogue to the WW production, the process can produce either a WZ (Fig. 5.4) or a ZZ (Fig.5.5) pair. Instead of the W bosons either one or two Z bosons are emitted which then decay into a lepton/ antilepton pair of the same generation, leading to a $\mu\tau$ final state with additional leptons. As the cross section for the Z production is way smaller then the of the W, in addition to the also small probability of a Z decaying leptonically [3], this processes are less important then the WW production.

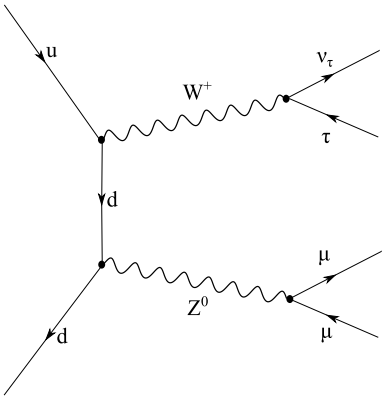

Fig. 5.4: Exemplary feynman diagram of the WZ pair production, where both bosons decay leptonically.

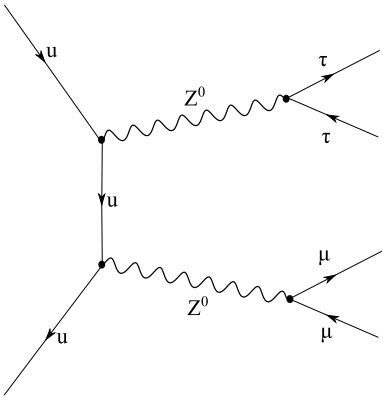

Fig. 5.5: Exemplary feynman diagram of the ZZ pair production, where both Z bosons decays into two leptons each.

Single top production

In this process a b quark absorbs a gluon and then decays before it can hadronize into a W boson and a top quark. The top quark decays furthermore into a b quark and another W boson. The final state is then similar to the WW pair production, including a $\mu\tau$ pair and a b-jet, as shown in Fig. 5.6.

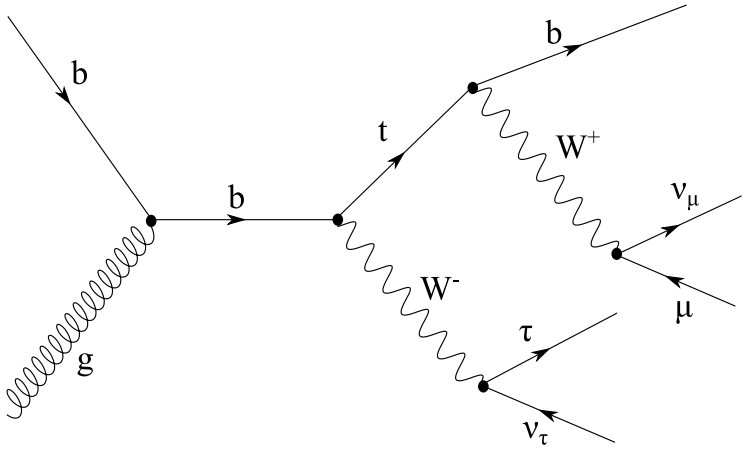

Fig. 5.6: Exemplary feynman diagram of the single top production, where a b quark absorbs a gluon and then decays into a W boson and a t quark, which further emits a W, and both W bosons decay leptonically into a $\mu\tau$ final state

5.3.2 Fake backgrounds

As the W and Z boson can also decay hadronically, additional diboson processes are taken in account as possible fake background. For example: If a W boson in the WW pair production decays into two quarks and the other decays into a muon + muon neutrino, a jet as result of the hadronization of the quarks can be misidentified as

tau and therefore a $\mu\tau$ final state is achieved. As muons need for reconstruction hits in the muon system (see chapter 4.2) and jets are rarely able to punch trough the hadronic calorimeter and the iron yoke, the probability of a jet to be misidentify as muon is small in comparison to a jet faking a tau. In addition muons can also be misidentified as τ leptons, which is for example important in the Drell-Yan process, if the Z decays into two muons.

W + jets process

In this process a W boson and an additional gluon are produced. While the W decays into a muon / muon neutrino, the gluon produces a jet which then can be misidentified as a tau, shown in Fig. 5.7.

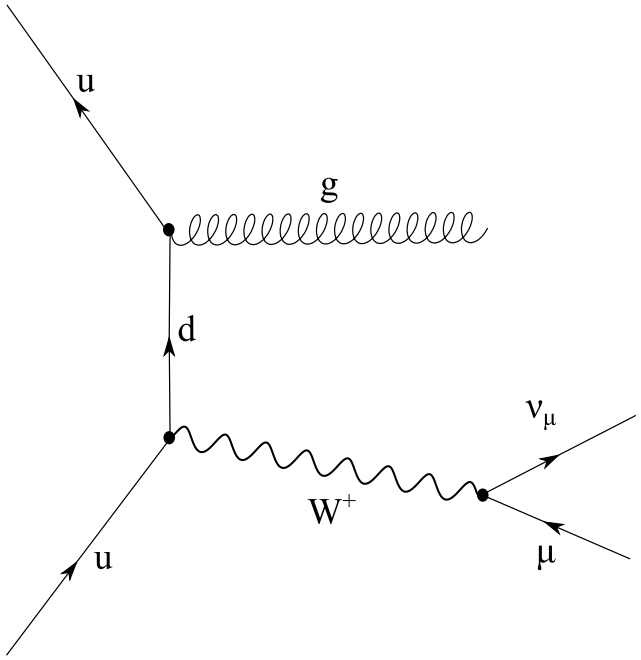

Fig. 5.7: Exemplary feynman diagram of the W + jets process. Here a W boson and a gluon are emitted, the W decays int a muon / muon neutrino and the gluon produces a jet faking a tau.

QCD process

Jets are particle streams which occur if quarks hadronize. A possible process where this happens is shown in Fig. 5.8 and is taken from the Quantum Chromodynamics (QCD).

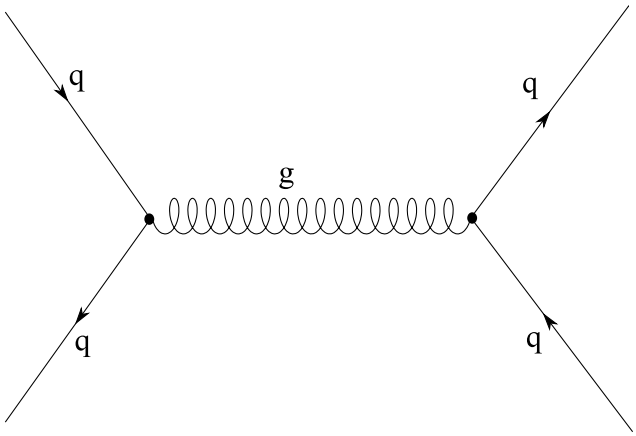

Fig. 5.8: Exemplary feynman diagram of a QCD process, where two quarks annihilate and emit a gluon, which further decays into two quarks. Both quarks hadronizes into jets.

6 Analysis

In this section different steps are taken to reduce the number of background events, while keeping the number of signal events high. Therefore the discriminators of the tau selection are studied and different kinematic cuts for the selected events are discussed. Furthermore quantities like the mass resolution, the signal efficiency and systematic uncertainties are analysed, as they are used for limit calculations.

6.1 Discriminators

The tau ID works in two steps: First the reconstruction of an τ_h candidate, which is done using the HPS algorithm. Second a set of discriminators is applied to separate τ_h decays from quark or gluon jets, from electrons and from muons to reduce the rate in which one of this particles/jets is misidentified as a τ_h. The discriminators are further given with different working-points [15]. As τ_h are mainly faked by jets, the isolation discriminator got more impact then the anti electron and anti muon. Therefore only the isolation is optimized and the other two are set to a loose working point to ensure a high efficiency later on. All discriminators and the reconstruction used are shown in Tab. 6.1.

Tab. 6.1: Used reconstruction and anti muon / anti electron, as well as all isolation discriminators looked at.

Reconstruction	*decayModeFinding* (HPS)
Anti muon	*againstMuonLoose3*
Anti electron	*againstElectronLooseMVA6*
Isolation	*byLooseCombinedIsolationDeltaBetaCorr3Hits*
	byMediumCombinedIsolationDeltaBetaCorr3Hits
	byTightCombinedIsolationDeltaBetaCorr3Hits
	byVLooseIsolationMVArun2v1BoldMwLT
	byLooseIsolationMVArun2v1BoldMwLT
	byMediumIsolationMVArun2v1BoldMwLT
	byTightIsolationMVArun2v1BoldMwLT
	byVTightIsolationMVArun2v1BoldMwLT

There are two different types of isolation discriminators in addition to the different working points. First there are the cut-based discriminators, which are indicated by an "DeltaBetaCorr" in their name. This isolation is computed by summing the transverse momenta of charge particles of $p_T > 0.5$ GeV and photons of $E_T > 0.5$ GeV within the isolation cone around the τ_h, excluding all charged hadrons which

are used to reconstruct the τ_h candidate.

Second there are multivariant ("MVA") isolation discriminators which combine the cut-based isolation with informations about the τ-lifetime. Therefore a Boosted Decision Tree (BDT) is used. This is a special algorithm which separates events in different categories, here either correct reconstructed or faked, based on different variables. These variables are, for example, the total numbers of photons in the event with $p_T > 5$ GeV , the tau flight distance for three-prong tau leptons or the χ^2 of the leading track.

The working-point of the particular isolation discriminator is given by: "VLoose" (very loose), "Loose", "Medium", "Tight", "VTight" (very tight).

To decide which isolation discriminator is the most optimal to use, two different quantities are taken in account: The efficiency (ϵ), as rate of correct reconstructed tau leptons passing the isolation, and the fake rate (f), as rate of quarks / gluons reconstructed as tau lepton passing the isolation.

A exact definition how the efficiency is computed is given in Eq. 6.1.

$$\epsilon = \frac{\mathrm{N}_\tau(p_T^{reco} > 20\,\mathrm{GeV}\ \&\ |\eta|^{reco} < 2.3\ \&\ \textit{decayModeFinding}\ \&\ \textit{isolation})}{\mathrm{N}_\tau(p_T^{reco} > 20\,\mathrm{GeV}\ \&\ |\eta|^{reco} < 2.3\ \&\ \textit{decayModeFinding})} \tag{6.1}$$

As definition, the ratio of the correctly reconstructed tau leptons which pass the isolation discriminator to all correctly reconstructed tau leptons is used. A tau counts as correctly reconstructed if it fulfils the reconstruction requirements ($p_T > 20$ GeV, $|\eta| < 2.3$ and *decayModeFinding*) and got a match with the visible part of an generator level tau (τ_{gen}^{vis}). For this matching criteria, a τ_{gen}^{vis} is taken in account if it got $p_T > 20$ GeV and $|\eta| < 2.3$ and in addition is in a $\Delta R < 0.5$ cone around the reconstructed tau (τ_{reco}). If there are two ore more matches, the generator level particle with the smallest ΔR to the reconstructed particle is chosen, as the efficiency is plotted as a function of p_T from the τ_{gen}^{vis}.

The fake rate is defined as shown in Eq. 6.2.

$$f = \frac{\mathrm{N}_\tau(p_T^{reco} > 20\,\mathrm{GeV}\ \&\ |\eta|^{reco} < 2.3\ \&\ \textit{decayModeFinding}\ \&\ \textit{isolation})}{\mathrm{N}_{q/g}(p_T^{gen} > 20\,\mathrm{GeV}\ \&\ |\eta|^{gen} < 2.3\ )} \tag{6.2}$$

Here the fake rate is the ratio of the number of falsely reconstructed tau leptons which pass the isolation discriminator to the overall number of generated quarks / gluons. The reconstruction requirements for the tau are identical to the efficiency and a tau lepton counts as falsely reconstructed if they got a $\Delta R < 0.5$ match to a generator level quark or gluon with $p_T > 20$ GeV and $|\eta| < 2.3$. Identical to the efficiency, the quark / gluon with the smallest ΔR is chosen as match, if there are

two or more particles within the cone, to plot the fake rate as function of p_T of the generated quarks / gluons.

For each different isolation discriminator the efficiency and fake rate are calculated, using different Monte Carlo samples: The Signal samples are used for the computation of the efficiency and the "QCD-MuEnrichted" background samples for the fake rate. The efficiencies for the different working points of the cut-based and MVA based discriminators are shown in Fig. 6.1 The fake rates are shown in Fig. 6.2.

To decide which isolation discriminator will be used in the analysis, the fake rate is plotted against the efficiency for each discriminator, shown in Fig. 6.3. The MVA based discriminators got smaller fake rates by the same efficiency in comparison to the cut-bases ones. Therefore a MVA based isolation is selected and as working-point the "Loose" discriminator is chosen. "Loose" was selected over "VLoose", as "VLoose" would have lead on the one hand to a improvement in the efficiency but on the other hand to a strong rise in the fake rate. Because of this, *byLooseIsolationMVArun2v1BoldMwLT* was chosen as isolation discriminator, as it has the best combination of high efficiency and small fake rate.

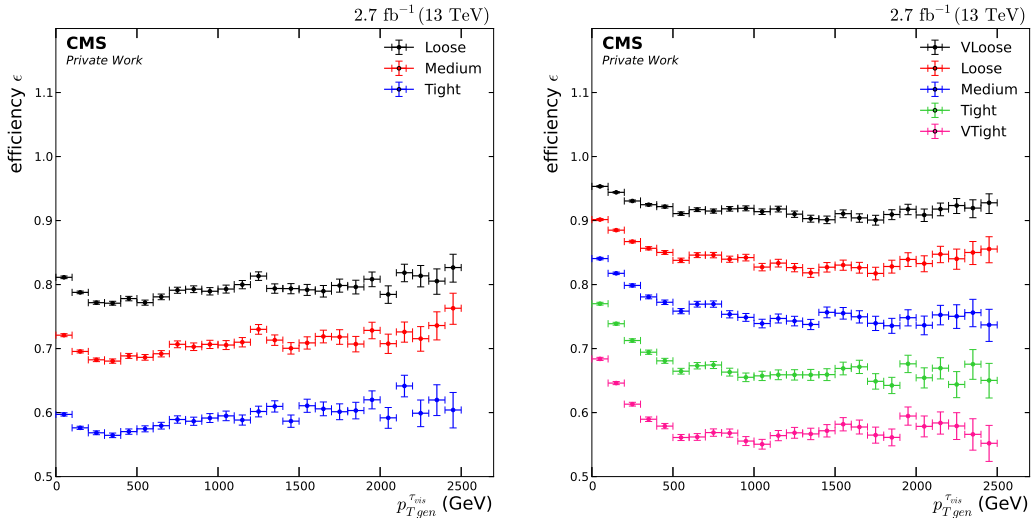

Fig. 6.1: Efficiencies for different working points of the cut-bases (left) and MVA based (right) discriminators

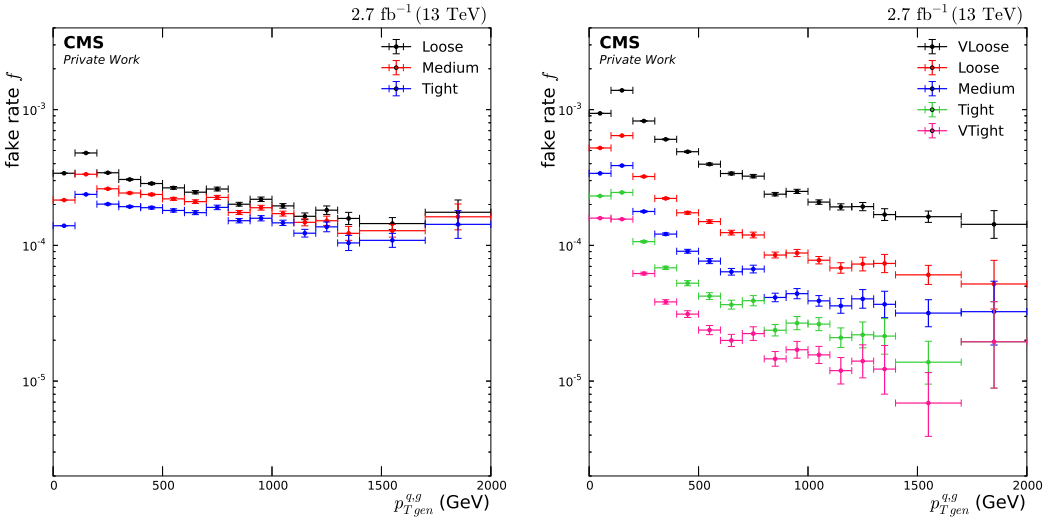

Fig. 6.2: Fake rates for different working points of the cut-bases (left) and MVA based (right) discriminators

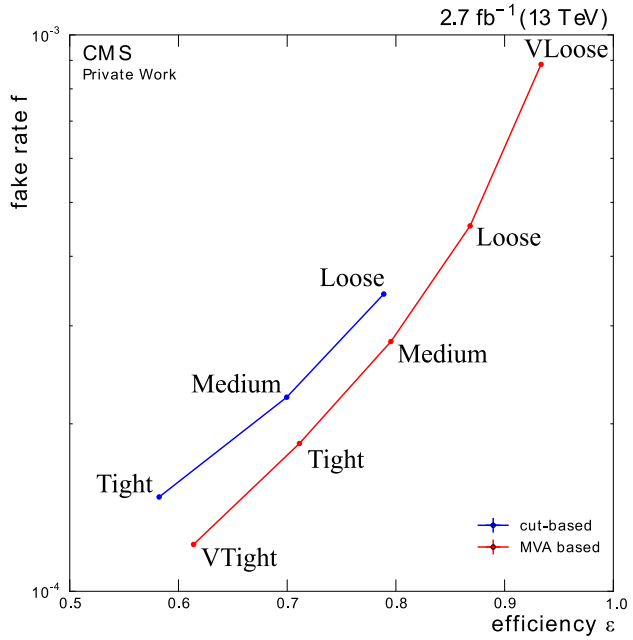

Fig. 6.3: Comparison of the different cut and MVA based isolation discriminators. The MVA based discriminators have got a lower fake rat at the same efficiency as the cut-based ones.

6.2 Mass Resolution

In this section the invariant mass resolution of the $\mu\tau$ pair is studied. Therefore the relative mass difference between the generated and the reconstructed $\mu\tau$ mass is computed. This is done for each mass bin of the Monte Carlo signal sample, using the final selection, where all kinematic cuts (discussed in section 6.6) are applied. The distributions are then fitted using a gaussian of the form $A \cdot exp\left(\frac{(x-B)^2}{2 \cdot C^2}\right)$ to obtain the width.

Examples for two different mass bins are shown in Fig. 6.4. The two plots show that the width of the distributions depends on the invariant $\mu\tau$ mass, therefore an additional plot which show the width in dependency of $M_{\mu\tau}$ is given in Fig. 6.5. The width for the 200 GeV sample is excluded, due to the low statistic in the histogram, which lead to a unrealistic fit. The dependency is fitted, as the mass resolution for arbitrary mass points is need in the limit calculation, which is done in later parts of the analysis. A function of the following form is used:

$$\sigma = \frac{A}{M_{\mu\tau}^{gen}} + B \cdot M_{\mu\tau}^{gen} + C \tag{6.3}$$

where $M_{\mu\tau}^{gen}$ is the invariant generator level mass of the $\mu\tau$ pair. The coefficients A, B, C are given in Fig. 6.5

The mass resolution is getting worse for high and for low masses, reaching a minimum at around 800 GeV. This is caused by different effect: First, the muon momentum resolution gets worse with high muon p_T. As the p_T of the muon gets higher, its trajectory becomes straighter and therefore is reconstructed with a higher error. Second, the resolution of the τ_h momentum gets extremely worse for small p_T. This is caused by the energy resolution of the HCAL, which also decreases for particles with low momentum. And third, the assumption of the tau neutrino having the same directing as the visible part of the tau decay is only viable for high p_T tau leptons. This leads to another decline of the mass resolution for small $M_{\mu\tau}$. The p_T resolution of muon and τ_h are shown in Fig. 6.6.

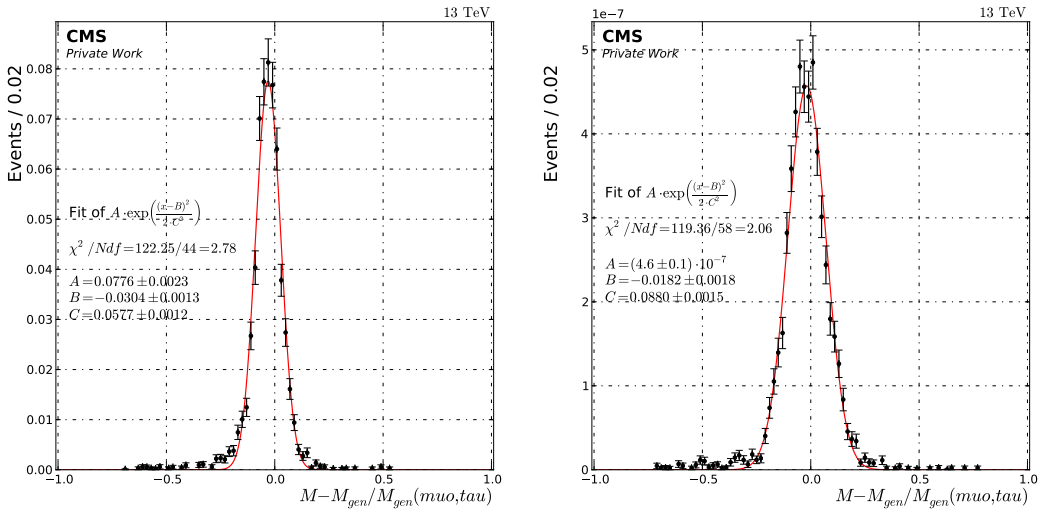

Fig. 6.4: Mass resolution for the $M_{\mu\tau} = 1000$ GeV sample with gaussian fit on the left and of the $M_{\mu\tau} = 5500$ GeV sample on the right

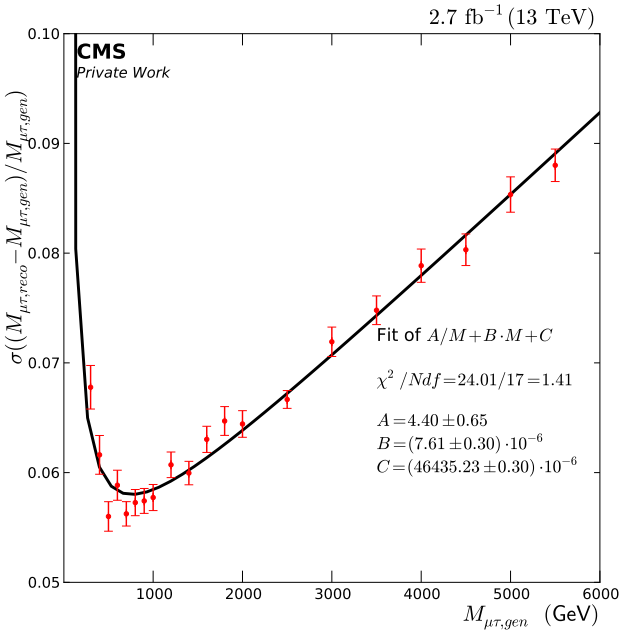

Fig. 6.5: Mass Resolution as a function of the invariant mass, which is worse for small and for high $M_{\mu\tau}$ and got a minimum at around 800 GeV.

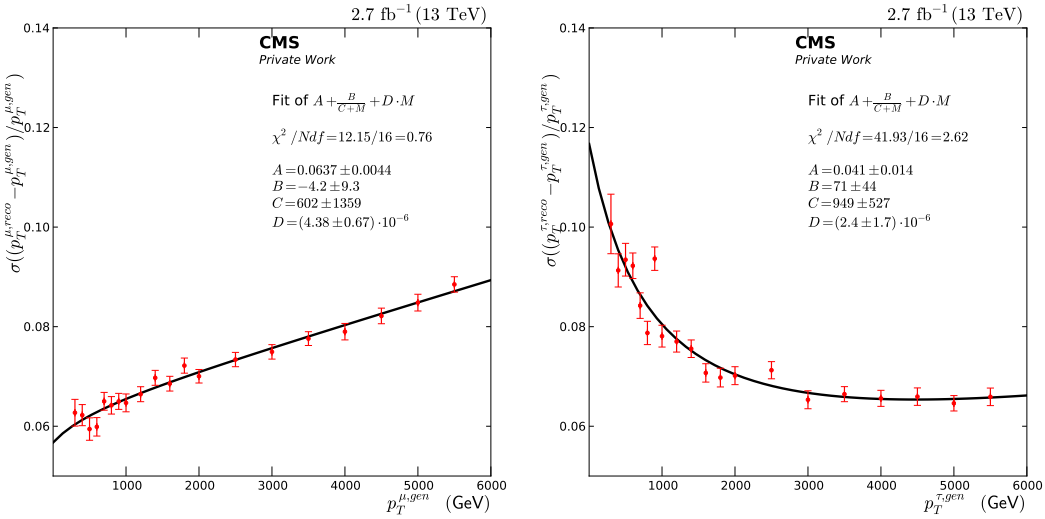

Fig. 6.6: The resolution of the transversal momentum of muon leptons (left) decreases with high muon p_T. The p_T resolution of the visible part of hadronic decaying tau leptons (right) is worse for small p_T.

6.3 Signal Efficiency

The signal efficiency is given in four different stages: Acceptance, trigger, selection and the final acceptance times efficiency. All efficiencies are calculated using only events which have on generator level a tau which decays hadronically, as well as a muon.

The acceptance is the rate of events with a generator level muon and a hadronic decaying tau within acceptance ($p_T^{\mu} > 53\,\text{GeV}$, $|\eta^{\mu}| < 2.4$, $p_T^{\tau} > 20\,\text{GeV}$, $|\eta^{\tau}| < 2.3$)

to all generated events with a muon and a hadronic decaying tau.
The trigger efficiency is given by the rate of events which fulfil the generator level acceptance requirements and furthermore pass the trigger, to all generated evens with a muon and a hadronic decaying tau.
For the selection efficiency, the events have to have a $\mu\tau$ resonance mass greater then zero in the reconstruction. The efficiency is the quotient of the number of these events to all generated events.
The final acceptance times efficiency is given by the rate of events which pass all kinematic cuts, described in section 6.6, to the total number of generated events. All four efficiencies are shown in Fig. 6.7.
All efficiencies are reasonably stable after the turn-on region, i.e. 1200 GeV. In this region the final efficiency of finding and reconstructing a $\mu\tau$ event within detector acceptance, which further passes all cuts, is above 25 %.
For the limit calculation the efficiency for arbitrary signal masses is needed. Therefore a fit is performed using the following function:

$$\epsilon = A + \frac{B}{C + M_{\mu\tau}^{gen}} + D \cdot M_{\mu\tau}^{gen} \tag{6.4}$$

The coefficients A, B, C, D are given in Fig. 6.7.

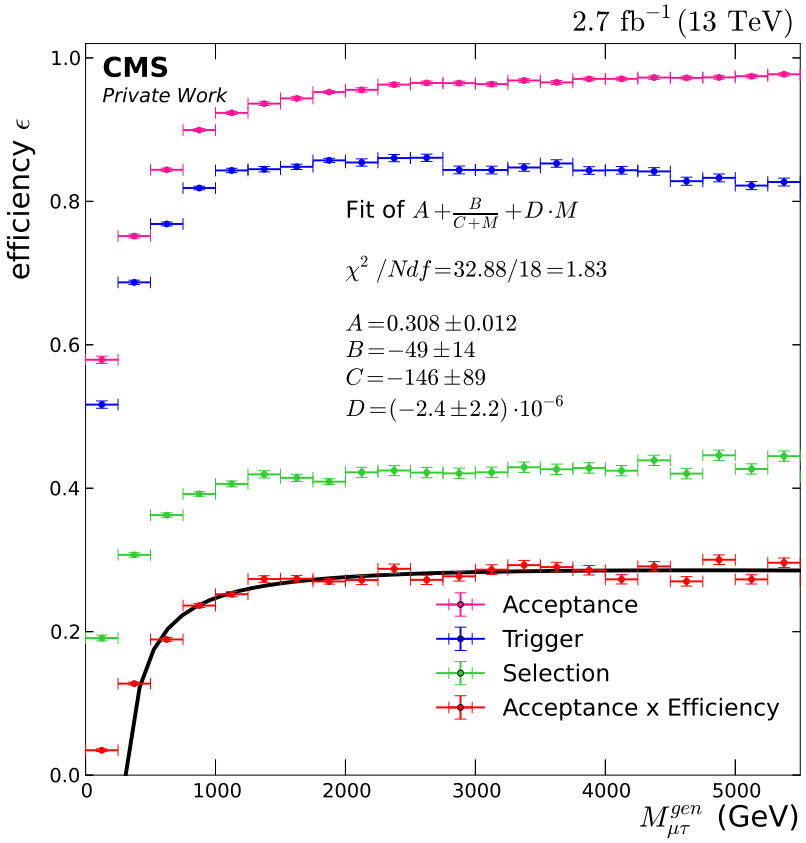

Fig. 6.7: Acceptance times efficiency of the RPV signal after final selection. The black curve is the fitted function used for the limit calculation

6.4 Systematics

There are different systematic uncertainties on the measurement of the transversal momentum of the muon and tau leptons. These are given by scale uncertainty for the muon and tau p_T, additional resolution uncertainty for the muon momentum and uncertainty resulting out of underlying events.
For the scale uncertainty, the muon momentum scale is shifted by 5 % per 1 TeV up and down and the tau momentum scale is shifted by 3 %.
The resolution uncertainty of the muon is estimated by smearing the momentum using a gaussian with a width of 3.2 %. To take underlying events in account, an additional uncertainty is used. This is estimated by a $\pm 5\,\%$ shift of the minimum bias cross section.

6.5 Limit calculation

There are two different limit types: Observed and expected. The observed limit is calculated by comparing data with the signal plus background model, while the expected limit compares simulated pseudoexperiments containing only background processes to the signal plus background model.
For both limit settings a Bayesion approach is used. In this the mass resolution, the signal efficiency and the invariant mass $M_{\mu\tau}$ distributions is used to calculate an upper limit on the section times branching ratio with a 95 % confidence level. In addition the listed systematics are taken in account, using the Markov-Chain Monte Carlo method. The full procedure is described in [17].
A multibin approach is used. In this not only the total number of background, signal and data events is taken in account, but also the signal and background shape. This is done using the multibin limit setting tool developed by the Higgs group [18].
All limits are calculated by Swagata Mukherjee.

6.6 Kinematic Cuts

In this section five different cuts are discussed: Opposite sign electric charge, b-jet veto, $\Delta\phi(\tau_h, E_T^{miss})$, $\Delta\phi(\tau_h, \mu)$ and M_T. These cuts are applied to improve the signal to background ratio. They are either theoretically motivated or by a different kinematic between signal and background processes.
The invariant $\mu\tau$ mass distribution without all cuts is shown in Fig. 6.8. There is a disagreement between data and background for small $M_{\mu\tau}$, caused by the jet-fake samples, which are inadequately produced. This could be solved by using a data

driven fake background estimation, which was not possible in the time frame of this thesis.

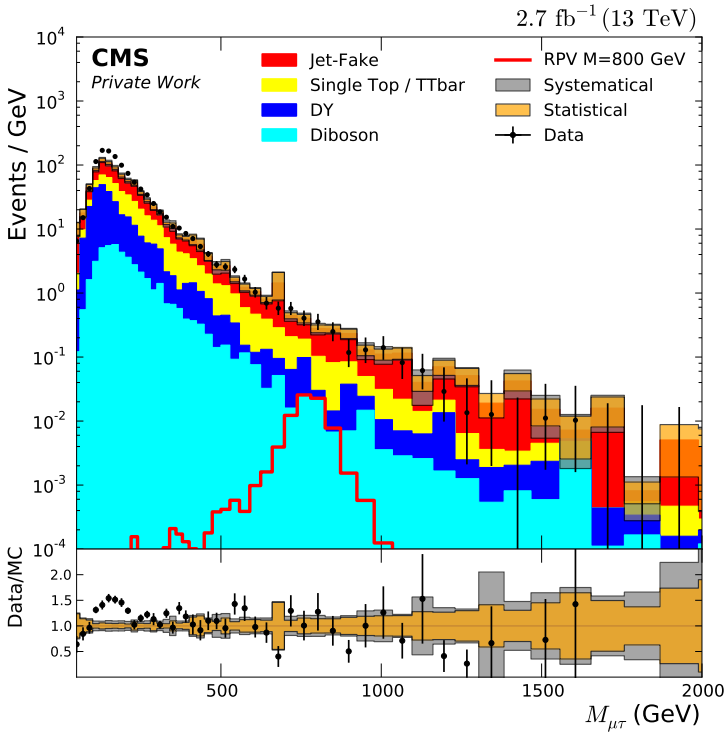

Fig. 6.8: Invariant $\mu\tau$ mass distribution without applied cuts. A $M_{\tilde{\nu}_\tau} = 500$ GeV signal sample is shown. There is a disagreement between data and background for small mass, caused by inadequately produced jet-fake samples.

While the theoretic motivated cuts got fixed cut values, the kinematic ones need to be optimised. This optimisation is done by calculating expected limits on the cross section of the signal for different cut values as described in section 6.5.

Opposite sign electric charge cut

In the signal mode, the muon and tau are produced with opposite electric charges, as the $\tilde{\nu}_\tau$ is electrically neutral. Therefore all events where the charge product of the $\mu\tau$ pair is greater 0 are vetoed. This cut reduces the fake background processes, as they produce a lot of same sign $\mu\tau$ pairs. As charge missreconstruction is only a small effect, most signal events pass this cut.

B-jet veto

Another theoretically motivated cut is on the number of b-jets. Therefore the *pfCombinedSecondaryVertexV2BJetTags* algorithm is used to identify a jet as b-jet. This

algorithm tries to reconstruct a pseudo secondary vertex, if there is none given in the event. Then, based on a set of variables, separates between b-jets and jets from other origins [19]. These variables are, for example, the flight distance significance in the transverse plane, the vertex mass or the number of tracks at the vertex.

As there are no b-jets in the signal model, all events with one or more b-jet are vetoed. In Fig. 6.9 a so called N-1 distribution of the number of b-jets is given. This distribution takes only the events in account which pass all other cuts. Therefore the impact of the studied cut can be estimated, ensuring that two cuts are not redundant. As seen in the N-1 plot, the main background processes reduced by this cut are $t\bar{t}$ and single top production.

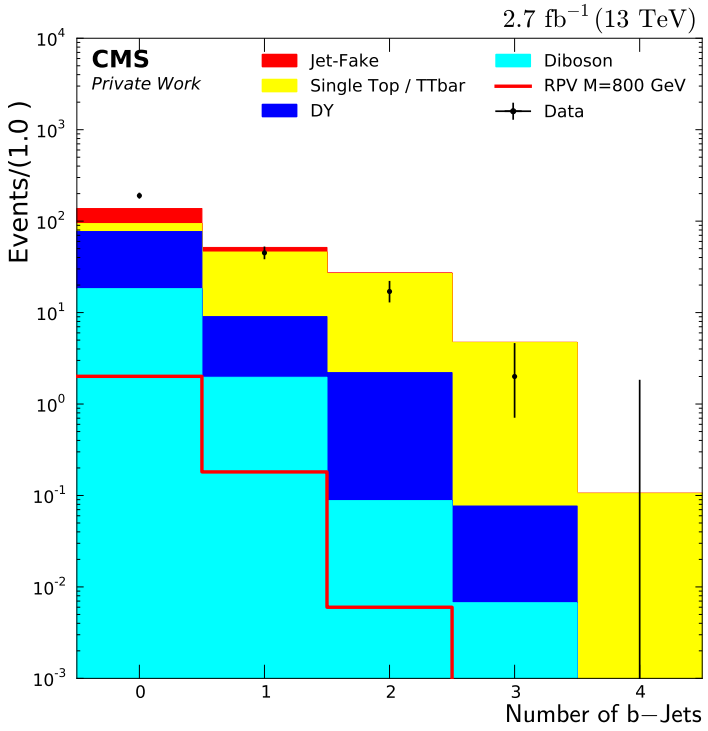

Fig. 6.9: N-1 distribution of the number of b-jets in the event. All events with one or more b-jets are vetoed, reducing the $t\bar{t}$ and single top background. The disagreement is caused by the poorly simulated jet-fake samples.

Cut on $\Delta\phi$ between τ_h and E_T^{miss}

In the signal model a high p_T tau is produced. If this tau decays hadonically, the visible part and the neutrino are strongly boosted in the same direction. The neutrino is not detectable and therefore is only measured as missing transversal energy. So the azimuth angle between the reconstructed τ_h and E_T^{miss} is expected to be small for the signal. For the background, a continuous distribution of the angle is expected, as this boost is not given. In addition, some processes produce more then one neutrino

and therefore have a resulting E_T^{miss} not pointing towards the direction of the visible tau products. In Fig. 6.10 the N-1 distribution of the azimuth angle between τ and E_T^{miss} is shown. The number of signal events got as expected a peak for small angle, different to the background.

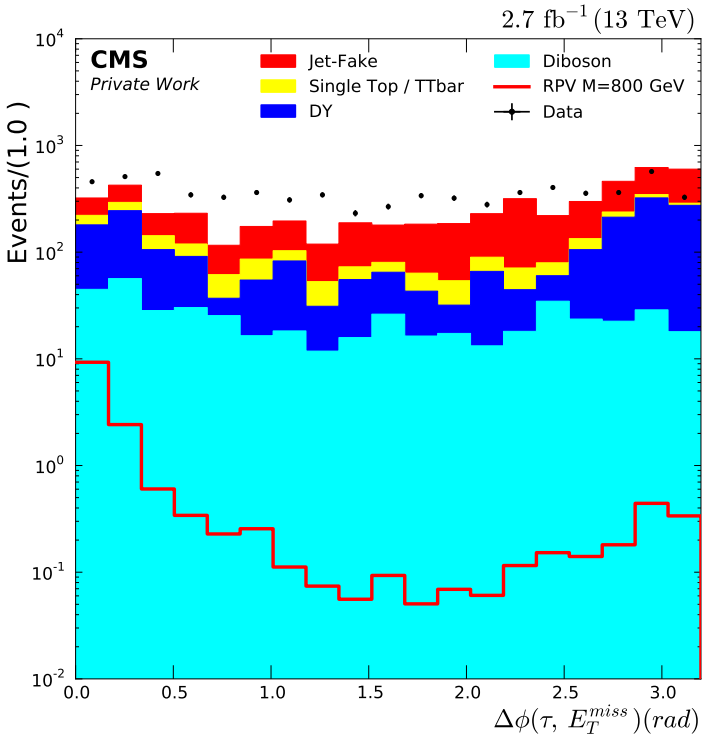

Fig. 6.10: N-1 distribution of the azimuth angle between τ and E_T^{miss}. For the signal the distribution got a peak at small angle, while the background got a continuously distributed angle. The disagreement between data and background is caused by the poorly simulated jet-fake samples.

To improve the signal to background ratio, all events with $\Delta\phi(\tau_h, E_T^{miss}) > \Delta\phi_{max}$ are discarded. To decide, which value to use for $\Delta\phi_{max}$, the expected limit on the cross section times branching ratio for three different signal masses (300 GeV, 1600 GeV, 3500 GeV) is calculated. This is done for ten different cut values covering a range from $\Delta\phi_{max} = 0.2$ to $\Delta\phi_{max} = 2$. The results are shown in Fig. 6.11.
Only the limits of the low 300 GeV signal mass change significantly with the chosen cut value. The limits on the medium and high signal mass only varies by 0.03 % (medium) and 0.02 % (high). Therefore the optimisation is done in respect to the low signal mass limits. The cut value with the lowest expected limit is chosen, resulting in a threshold of $\Delta\phi_{max} = 0.4$ for this cut.

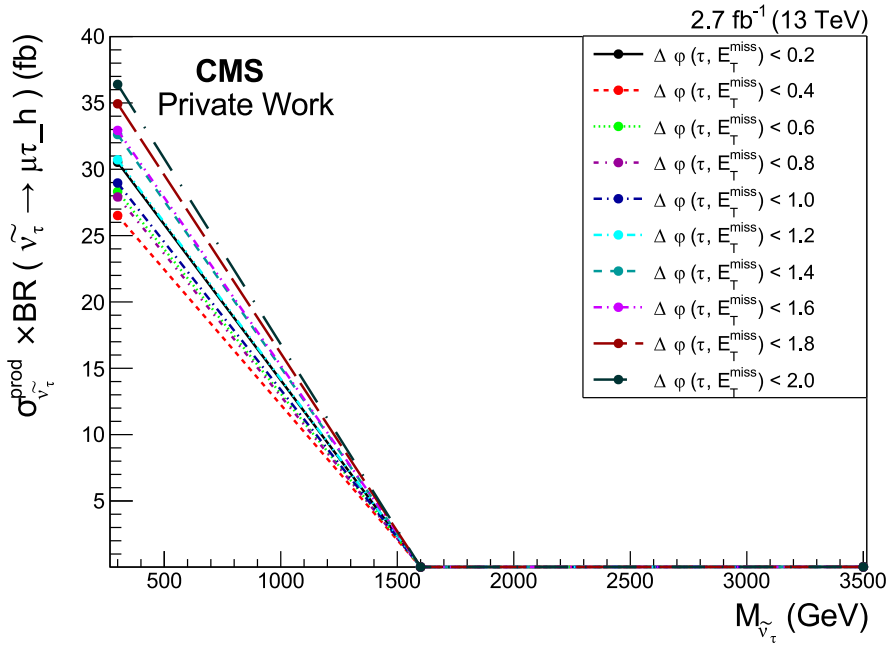

Fig. 6.11: Expected limits of ten different $\Delta\phi_{max}$ values for a low, a medium and a high signal mass. Only the low mass limits are significantly influenced by the cut values. The optimal cut value, the value with the lowest limit, is $\Delta\phi_{max} = 0.4$

Cut on $\Delta\phi$ between τ_h and μ

In the rest frame of the $\tilde{\nu}_\tau$, the muon and the tau are produced back to back. In assumption that the τ_h is strongly boosted in the initial tau direction, the azimuth angle between the τ_h and the muon is expected to be π in the signal model. This holds not true for the background, as there is no preferred angle. The N-1 distribution of the azimuth angle between the τ_h and the muon is shown in Fig. 6.12. The dependency of the signal shows as expected a peak for angle close to π, while the background shows only a slight dependency on $\Delta\phi$.
The artefact at $\Delta\phi = 0.75$ is caused by a characteristic of the generator used to produce the Drell-Yan samples: The MC@LNO generator produces negative events to take destructive interferences in account [20].

To separate background from signal, all events with $\Delta\phi(\tau_h, \mu) < \Delta\phi_{min}$ are vetoed. Similar to the $\Delta\phi(\tau_h, E_T^{miss})$ cut, the threshold $\Delta\phi_{min}$ is optimised calculating limits for three signal mass points and for ten different cut values. The cut values cover a range from $\Delta\phi_{min} = 1.3$ to $\Delta\phi_{min} = 3.1$. The results are shown in Fig. 6.13. The optimisation is done using the limits of the low signal mass, analogous to the $\Delta\phi(\tau_h, E_T^{miss})$ cut. This leads to an optimal threshold of $\Delta\phi_{min} = 2.9$.

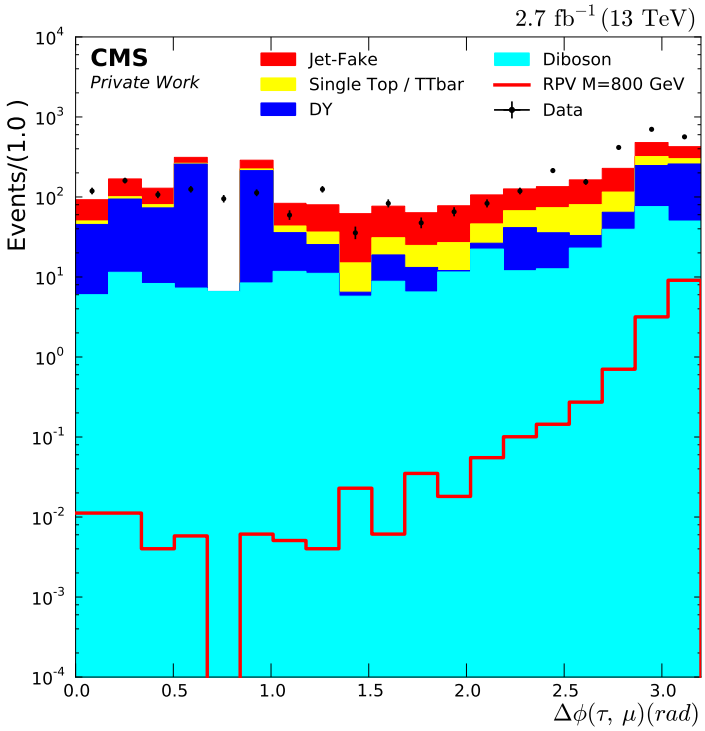

Fig. 6.12: N-1 distribution of the azimuth angle between τ and μ. For the signal the distribution got a peak around $\Delta\phi = \pi$, while the background got a continuously distributed angle. The disagreement is caused by the poorly simulated jet-fake samples.

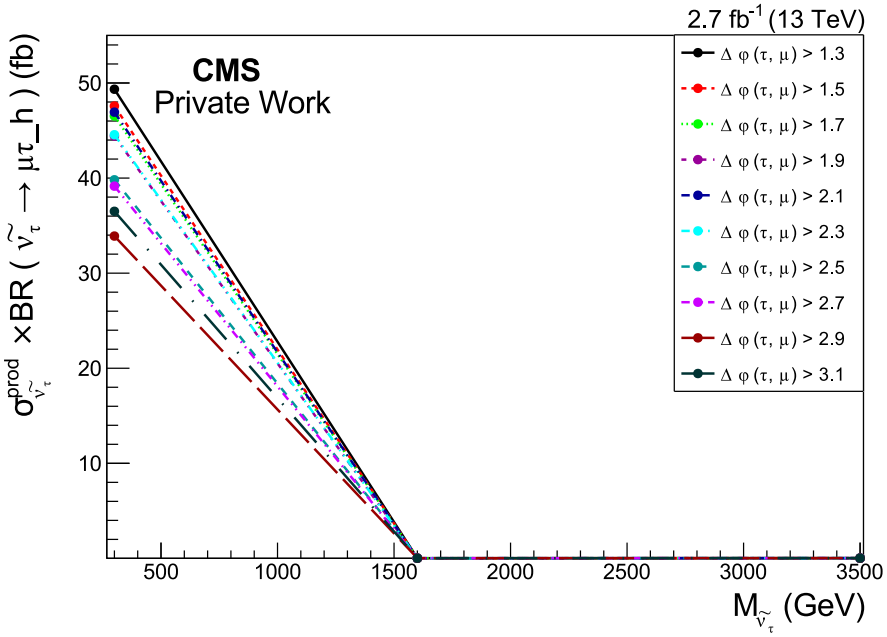

Fig. 6.13: Expected limits of ten different $\Delta\phi_{min}$ values for a low, a medium and a high signal mass. Only the low mass limits are significantly influenced by the cut values. The optimal cut value, the value with the lowest limit, is $\Delta\phi_{min} = 2.9$

Transverse mass between μ and E_T^{miss}

An additional cut on the transverse mass M_T between μ and the transverse missing energy is applied. M_T is defined as:

$$M_T = \sqrt{2p_T^{\mu} E_T^{miss}(1 - \cos(\Delta\phi))} \tag{6.5}$$

where $\Delta\phi$ is the azimuth angle between the muon momentum and the E_T^{miss}. The N-1 distribution of M_T is shown in Fig. 6.14.

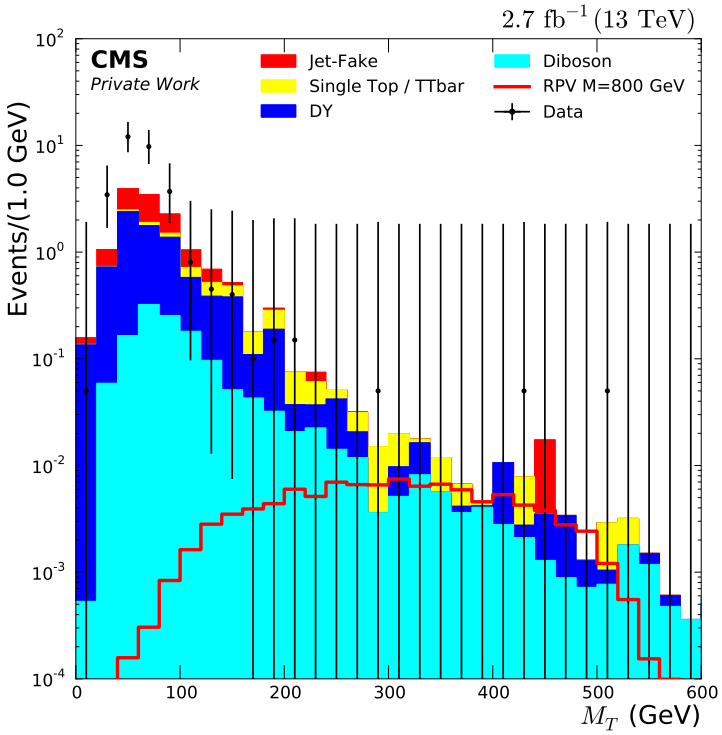

Fig. 6.14: N-1 distribution of M_T. As the shapes of the distributions are different for background and signal, a M_T^{min} threshold is used to improve the signal to background ratio. The disagreement is caused by the poorly simulated jet-fake samples.

The shapes of the background and the signal distributions differ: The background got a strong peak around the W mass and then drops quickly, while the signal got a near constant, expanded plateau. To utilize this difference, a lower threshold to the transverse mass M_T^{min} is set and optimized. This is done by the same procedure as in the $\Delta\phi$ cuts. The ten cut values cover a range from $M_T^{min} = 70\,\text{GeV}$ to $M_T^{min} = 270\,\text{GeV}$.
The results of the limit calculations are shown in Fig. 6.15. As the expected limits differs in a width range for the low signal mass, an additional plot is done. This plot shows the expected limit in dependency of M_T^{min}, seen in Fig. 6.16. The optimal value is $M_T^{min} = 70\,\text{GeV}$.

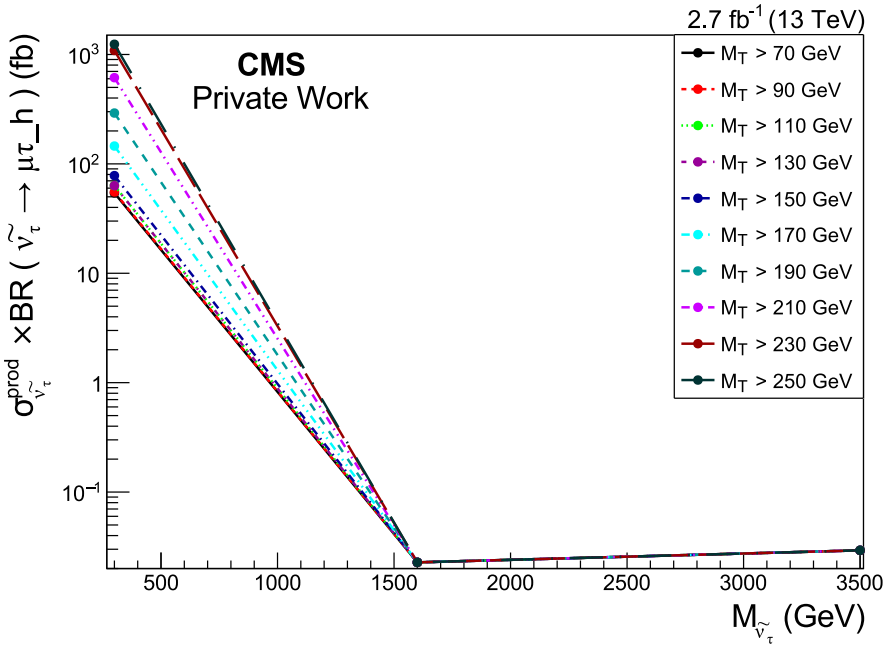

Fig. 6.15: Expected limits of ten different M_T^{min} values for a low, a medium and a high signal mass. Only the low mass limits are significantly influenced by the cut values.

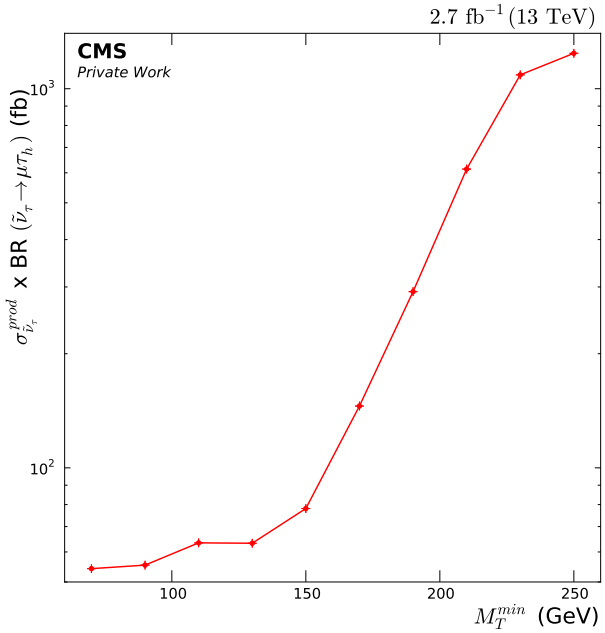

Fig. 6.16: Expected limits for the 300 GeV signal mass, in dependency of M_T^{min}. The optimal cut value, the value with the lowest limit, is $M_T^{min} = 70\,\text{GeV}$

Summary and cut flow

A summary of all used cuts and the optimised thresholds is given in Tab. 6.2. In addition the cut flow is given in Fig. 6.17, showing the number of events after each cut. After all cuts, the number of background events is reduced to 0.81%, while the number of signal events is only reduced to 59% (for the $M_{\tilde{\nu}_\tau} = 800\,\text{GeV}$ signal sample).

Tab. 6.2: All cuts and the used thresholds

Cut	Cut value
Opp. sign el. charge	$q_\mu \cdot q_{\tau_h} < 0$
B-jet veto	Number of b-jets < 1
$\Delta\phi(\tau_h, E_T^{miss})$	$\Delta\phi_{max} = 0.4$
$\Delta\phi(\tau_h, \mu)$	$\Delta\phi_{min} = 2.9$
Transverse mass	$M_T^{min} = 70\,\text{GeV}$

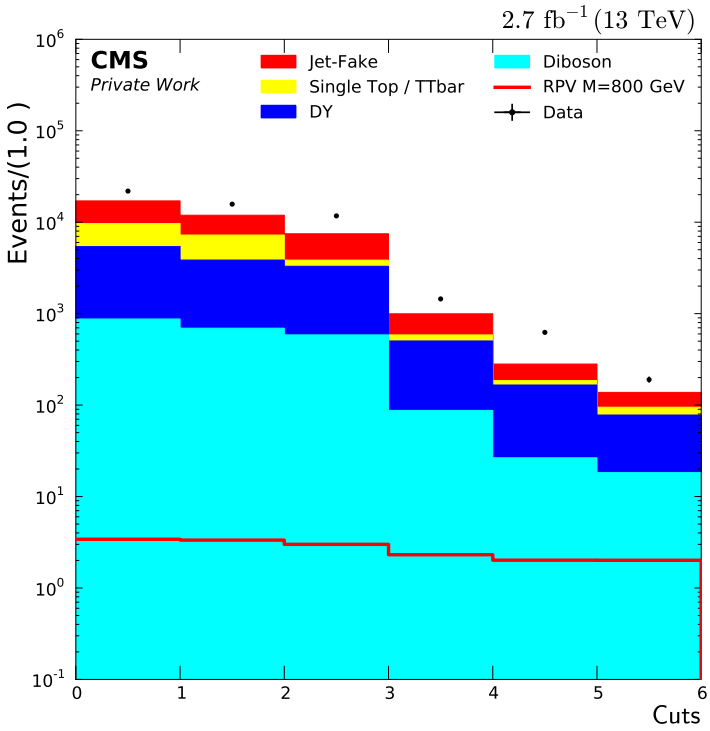

Fig. 6.17: In the cut flow the number of events after each applied cut is given. The background gets strongly reduce, while the number of signal events is only slightly decreased.

7 Result

The invariant mass distribution after all cuts are applied is shown in Fig. 7.1.

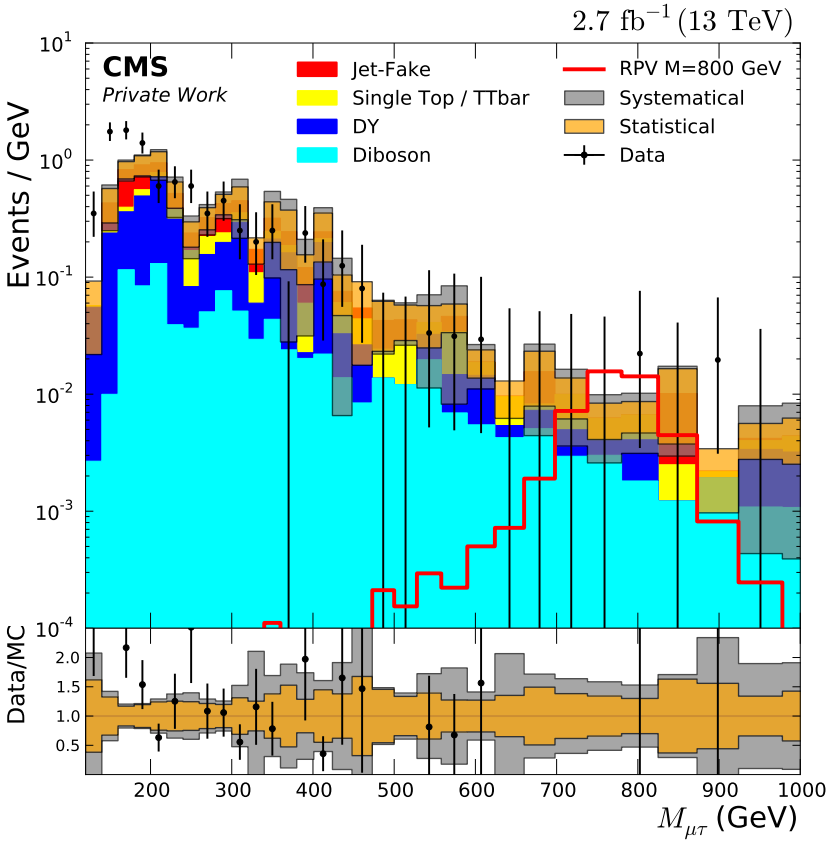

Fig. 7.1: Invariant $\mu\tau$ mass distribution after all cuts are apllied. A $M_{\tilde{\nu}_\tau} = 500$ GeV signal sample is shown. There is a disagreement between data and background for small mass, caused by inadequately produced jet-fake samples. Except for this, no other excess of data over background events is seen.

The excess at low masses is given by the inadequate simulated jet-fake samples. Outside of this region, no excess in respect to the expectation is found. Therefore a 95% confidence level (CL) exclusion limit on the signal cross section is calculated as discussed in section 6.5. The expected and observed limit are shown in Fig. 7.2.
For RPV couplings $\lambda'_{311} = \lambda_{233} = 0.01$, a lower limit on the $\tilde{\nu}_\tau$ mass of 720 GeV is obtained. At the moment there is no other analysis of the $\mu\tau$ channel using $\sqrt{s} = 13$ TeV data to compare this limit. Therefore a comparison to the Atlas result, using $\sqrt{s} = 8$ TeV data with an integrated luminosity of 20.3 fb^{-1}, is done [21].
As different coupling are used by Atlas for the RPV signal ($\lambda'_{311} = 0.11$ and $\lambda_{233} = 0.07$), the mass limits are not comparable. To solve this, the mass limit of this

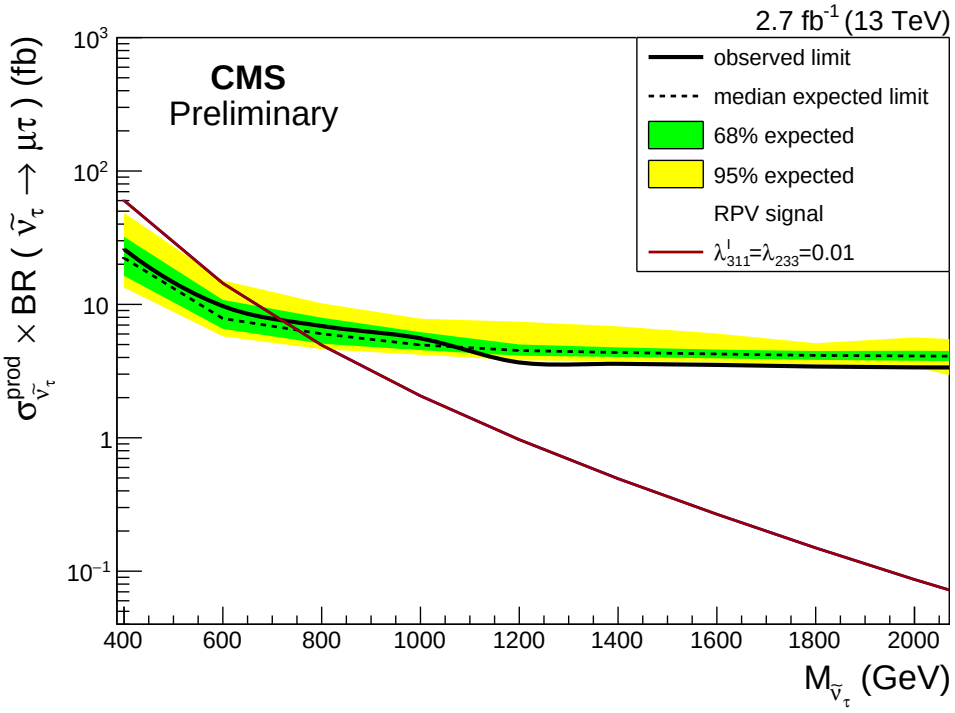

Fig. 7.2: Expected and observed cross section limits in dependency of the $\tilde{\nu}_\tau$ mass are given by the black dotted and solid line. The signal cross section using the RPV couplings $\lambda'_{311} = \lambda_{233} = 0.01$ are given by the red line.

analysis could be scaled to the parameters used in the Atlas paper. This was not possible due to the time frame of this thesis.

The expected limits of both results are compared. The expected is chosen over the observed limit, to exclude the statistical fluctuations of the data. For different mass points, the expected cross section times branching ratio limit is given in Tab. 7.1. For hight masses the expected limit of this analysis is higher then of the Atlas results.

Tab. 7.1: Expected limits ($\sigma^{prod}_{\tilde{\nu}_\tau}$ x BR $(\tilde{\nu}_\tau \to \mu\tau)$ (fb)) for different mass points compared between the Atlas results and the results of this thesis.

$M_{\tilde{\nu}_\tau}$ (GeV)	Thesis at 13 TeV (fb)	Atlas at 8 TeV (fb)
500	15	60
1000	7.5	5
1500	5	2.5
2000	4	2

8 Conclusion

A search for the resonant production of a tau sneutrino decaying into a $\mu\tau_h$ pair has been carried out. For this, 2.7 fb^{-1} of CMS data taken in 2015 with a center of mass energy of 13 TeV has been used. The tau events selection criteria where discussed and chosen. Several cuts were studied and applied to improve the signal to background ratio. With the exception of inadequate simulated jet-fake samples, which causes a disagreement at low mass regions, no significant excess in data compared to the SM background has been observed.
A mass limit of 720 GeV is set on the resonant production of a tau sneutrino in RPV SUSY, which decays into a muon and a hadronic decaying tau.

9 Appendix

Tab. 9.1: List of all used Monte Carlo background samples with an actual $\mu\tau$ final state. For each sample the generator, kinematic cuts, cross section and the number of events are given.

Process	Generator	Binning [GeV]	Cross section [pb]	N_{events}
DY $\rightarrow \tau\tau$	Madgraph	$50 < M_{ll}$	6020	8961180
DY $\rightarrow \tau\tau$	MC@LNO	$100 < M_{ll} < 200$	226	101927
DY $\rightarrow \tau\tau$	MC@LNO	$200 < M_{ll} < 400$	7.7	894280
DY $\rightarrow \tau\tau$	MC@LNO	$400 < M_{ll} < 500$	0.42	10745
DY $\rightarrow \tau\tau$	MC@LNO	$500 < M_{ll} < 700$	0.24	10077
DY $\rightarrow \tau\tau$	MC@LNO	$700 < M_{ll} < 800$	0.035	10208
DY $\rightarrow \tau\tau$	MC@LNO	$800 < M_{ll} < 1000$	0.03	9916
DY $\rightarrow \tau\tau$	MC@LNO	$1000 < M_{ll} < 1500$	0.016	9432
DY $\rightarrow \tau\tau$	MC@LNO	$1500 < M_{ll} < 2000$	0.002	9692
DY $\rightarrow \tau\tau$	MC@LNO	$2000 < M_{ll} < 3000$	0.00054	9061
t	Powheg	-	42	3089200
$\bar{t}$	Powheg	-	25.3	1630900
tW	Powheg	-	36	1000000
$\bar{t}$W	Powheg	-	36	999400
$t\bar{t}$	Powheg	-	832	97958042
$t\bar{t}$	Powheg	$700 < M_{t\bar{t}} < 1000$	77	3041206
$t\bar{t}$	Powheg	$1000 < M_{t\bar{t}}$	21	1782160
WW $\rightarrow 2l2\nu$	Powheg	-	12	1979988
WW $\rightarrow 2l2\nu$	Powheg	$200 < M_{ll} < 600$	1.4	200000
WW $\rightarrow 2l2\nu$	Powheg	$600 < M_{ll} < 1200$	0.057	200000
WW $\rightarrow 2l2\nu$	Powheg	$1200 < M_{ll} < 2500$	$3.6 \cdot 10^{-3}$	19440
WW $\rightarrow 2l2\nu$	Powheg	$2500 < M_{ll}$	$5.4 \cdot 10^{-5}$	38969
ZZ $\rightarrow 4l$	MC@LNO	-	1.2	10747136
WZ $\rightarrow 3l\nu$	Powheg	-	4.4	200000

Tab. 9.2: List of all used Monte Carlo fake background samples. For each sample the generator, possible binning, cross section and the number of events is given.

Process	Generator	Binning [GeV]	Cross section [pb]	N_{events}
Z $\rightarrow \mu\mu$	Powheg	$50 < M_{ll} < 120$	1975	297200
Z $\rightarrow \mu\mu$	Powheg	$120 < M_{ll} < 200$	19	100000
Z $\rightarrow \mu\mu$	Powheg	$200 < M_{ll} < 400$	2.7	100000
Z $\rightarrow \mu\mu$	Powheg	$400 < M_{ll} < 800$	0.24	99600
Z $\rightarrow \mu\mu$	Powheg	$800 < M_{ll} < 1400$	0.017	97600
Z $\rightarrow \mu\mu$	Powheg	$1400 < M_{ll} < 2300$	0.0014	99200
Z $\rightarrow \mu\mu$	Powheg	$2300 < M_{ll} < 3500$	$8.9 \cdot 10^{-5}$	100000
Z $\rightarrow \mu\mu$	Powheg	$3500 < M_{ll} < 4500$	$4.1 \cdot 10^{-6}$	57114
Z $\rightarrow \mu\mu$	Powheg	$4500 < M_{ll} < 6000$	$4.6 \cdot 10^{-7}$	100000
Z $\rightarrow \mu\mu$	Powheg	$6000 < M_{ll}$	$2.1 \cdot 10^{-8}$	99200
W+jets $\rightarrow l\nu$	Madgraph	-	61528	47161328
W+jets $\rightarrow l\nu$	Madgraph	$100 < HT < 200$	1627	10205377
W+jets $\rightarrow l\nu$	Madgraph	$200 < HT < 400$	435	4900732
W+jets $\rightarrow l\nu$	Madgraph	$400 < HT < 600$	59	1943664
W+jets $\rightarrow l\nu$	Madgraph	$600 < HT < 800$	15	3767766
W+jets $\rightarrow l\nu$	Madgraph	$800 < HT < 12000$	6.7	48924
W+jets $\rightarrow l\nu$	Madgraph	$1200 < HT < 2500$	1.6	246239
W+jets $\rightarrow l\nu$	Madgraph	$2500 < HT$	0.039	251982
W+$\gamma \rightarrow l\nu$	Madgraph	-	489	610226
W+$\gamma \rightarrow l\nu$	Madgraph	$p_{T_\gamma} < 500$	0.011	1390140
Z+$\gamma \rightarrow 2lG$	MC@LNO	-	118	4424816
WW $\rightarrow l\nu qq$	Powheg	-	50	360629
WW $\rightarrow 4q$	Powheg	-	52	2000000
ZZ $\rightarrow 2l2q$	MC@LNO	-	3.2	15256630
ZZ $\rightarrow 2l2\nu$	Powheg	-	0.56	8707880
ZZ $\rightarrow 4q$	MC@LNO	-	6.8	29608039
WZ $\rightarrow l3\nu$	MC@LNO	-	3.0	1703772
WZ $\rightarrow 2l2q$	MC@LNO	-	5.6	25211777
QCD-MuEnrichted	Pythia8	$30 < p_T < 50$	1652471	29866852
QCD-MuEnrichted	Pythia8	$50 < p_T < 80$	437504	20378392
QCD-MuEnrichted	Pythia8	$80 < p_T < 120$	106034	13749024
QCD-MuEnrichted	Pythia8	$120 < p_T < 170$	25191	7971018
QCD-MuEnrichted	Pythia8	$170 < p_T < 300$	8654	7910182
QCD-MuEnrichted	Pythia8	$300 < p_T < 470$	797	7845620
QCD-MuEnrichted	Pythia8	$470 < p_T < 600$	79	3841262
QCD-MuEnrichted	Pythia8	$600 < p_T < 800$	25	2483256
QCD-MuEnrichted	Pythia8	$800 < p_T < 100$	4.7	3661059
QCD-MuEnrichted	Pythia8	$1000 < p_T$	1.6	3938782

Acknowledgement

First I want to thank my surveyor Prof. Dr. Hebbeker for making this highly interesting bachelor thesis possible. Additionally i want to thank Prof. Dr. Feld, not only for being my second surveyor, but also for arousing my interest in Particle Physics with his lectures.
Also i want to thank the members of the Aachen CMS IIIA group for the interesting insights into current research, as well as the help for every problem. In special, i want to thank my tutor Sören Erdweg, who spend his time answering my countless questions, proof read my thesis and overall supported me during the whole work on this thesis.
Also i want to thank Swagata Mukherjee for calculating all limits and her helpful tips.
In addition, i want thank Alex Kreuzer and Jonas Lieb for the great working atmosphere and the constructive discussions. At last i want to thank my family and friends for the moral support during the whole study and all the help i got from them.

Bibliography

[1] Wolfgang Demtröder. *Experimentalphysik 4*. Springer Berlin Heidelberg, 2014 (cit. on p. 3).

[2] Christoph Berger. *Teilchenphysik*. Springer Berlin Heidelberg, 1992 (cit. on p. 3).

[3] K.A. Olive. „Review of Particle Physics“. In: *Chinese Phys. C* 38.9 (90001(2014)), p. 090001 (cit. on pp. 4, 5, 7, 14, 20).

[4] Serguei Chatrchyan et al. „Observation of a new boson at a mass of 125 GeV with the CMS experiment at the LHC“. In: *Phys. Lett.* B716 (2012), pp. 30–61. arXiv: 1207.7235 [hep-ex] (cit. on p. 5).

[5] K. Abe, J. Adam, H. Aihara, et al. „Measurements of neutrino oscillation in appearance and disappearance channels by the T2K experiment with 6.6×10^{20} protons on target“. In: *Phys. Rev. D* 91 (7 2015), p. 072010 (cit. on p. 5).

[6] Stephen P. Martin. „A Supersymmetry primer“. In: (1997). [Adv. Ser. Direct. High Energy Phys.18,1(1998)]. arXiv: hep-ph/9709356 [hep-ph] (cit. on p. 6).

[7] Ian J. R. Aitchison. „Supersymmetry and the MSSM: An Elementary introduction“. In: (2005). arXiv: hep-ph/0505105 [hep-ph] (cit. on p. 6).

[8] R. Barbier, C. Bérat, M. Besançon, et al. „R-Parity-violating supersymmetry“. In: *Physics Reports* 420.1-6 (2005), pp. 1–195 (cit. on p. 7).

[9] Herbi K. Dreiner, Jong Soo Kim, and Marc Thormeier. „A Simple baryon triality model for neutrino masses“. In: (2007). arXiv: 0711.4315 [hep-ph] (cit. on p. 7).

[10] The CMS Collaboration, S Chatrchyan, G Hmayakyan, et al. „The CMS experiment at the CERN LHC“. In: *J. Inst.* 3.08 (2008), S08004–S08004 (cit. on p. 9).

[11] Muon POG. *Muon ID*. https://twiki.cern.ch/twiki/bin/view/CMS/SWGuideMuonIdRun2 (cit. on p. 13).

[12] G. Abbiendi et al. „Muon Reconstruction in the CMS detector“. CMS AN-2008/097 (cit. on p. 13).

[13] Yuta Takahashi et al. „Tau reconstruction and identification performance in run 2“. CMS AN-15-229 (cit. on p. 14).

[14] The CMS collaboration. „Reconstruction and identification of tau lepton decays to hadrons and nu tau at CMS“. In: *Journal of Instrumentation* 11.01 (2016), P01019 (cit. on p. 14).

[15]Tau POG. *Tau ID*. https://twiki.cern.ch/twiki/bin/viewauth/CMS/ TauIDRecommendation13TeV (cit. on pp. 14, 25).

[16]Alexander Belyaev, Neil D Christensen, and Alexander Pukhov. „CalcHEP 3.4 for collider physics within and beyond the Standard Model“. In: *Computer Physics Communications* 184.7 (2013), pp. 1729–1769 (cit. on p. 17).

[17]Soeren Erdweg; Andreas Gueth; Thomas Hebbeker; Henning Keller; Arnd Meyer; and Swagata Mukherjee. „Search for lepton flavour violating decays of heavy resonances to e mu pairs in pp collisions at sqrt(s) = 13 TeV“. AN2015-191 (cit. on p. 32).

[18]Higgs working group. *Higgs combined limit setting tool*. https://twiki.cern.ch/twiki/bin/view/CMS/SWGuideHiggsAnalysisCombinedLimit (cit. on p. 32).

[19]The CMS collaboration. „Identification of b-quark jets with the CMS experiment“. In: *J. Inst.* 8.04 (2013), P04013–P04013 (cit. on p. 34).

[20]Stefano Frixione and Bryan R. Webber. „The MC@NLO event generator“. In: (2002). arXiv: hep-ph/0207182 [hep-ph] (cit. on p. 36).

[21]Georges Aad et al. „Search for a Heavy Neutral Particle Decaying to $e\mu$, $e\tau$, or $\mu\tau$ in pp Collisions at $\sqrt{s} = 8$ TeV with the ATLAS Detector“. In: *Phys. Rev. Lett.* 115.3 (2015), p. 031801. arXiv: 1503.04430 [hep-ex] (cit. on p. 41).